Vol.5, March.2014 ISSN 2354-7065

Journal of Ocean, Mechanical and Aerospace

-Science and Engineering-

ISOMAse

International Society of Ocean, Mechanical and Aerospace, Scientists and Engineers

Journal of Ocean, Mechanical and Aerospace
-Science and Engineering-
Vol.5: March 2014

Contents

ISOMAse

International Society of Ocean, Mechanical and Aerospace
-Scientists and Engineers-

Journal of Ocean, Mechanical and Aerospace
-Science and Engineering-
Vol.5: March 2014

About JOMAse

The **Journal of Ocean, Mechanical and Aerospace -science and engineering- (JOMAse, ISSN: 2354-7065)** is an online professional journal which is published by the International Society of Ocean, Mechanical and Aerospace -scientists and engineers- (ISOMAse), Insya Allah, twelve volumes in a year. The mission of the JOMAse is to foster free and extremely rapid scientific communication across the world wide community. The JOMAse is an original and peer review article that advance the understanding of both science and engineering and its application to the solution of challenges and complex problems in naval architecture, offshore and subsea, machines and control system, aeronautics, satellite and aerospace. The JOMAse is particularly concerned with the demonstration of applied science and innovative engineering solutions to solve specific industrial problems. Original contributions providing insight into the use of computational fluid dynamic, heat transfer, thermodynamics, experimental and analytical, application of finite element, structural and impact mechanics, stress and strain localization and globalization, metal forming, behaviour and application of advanced materials in ocean and aerospace engineering, robotics and control, tribology, materials processing and corrosion generally from the core of the journal contents are encouraged. Articles preferably should focus on the following aspects: new methods or theory or philosophy innovative practices, critical survey or analysis of a subject or topic, new or latest research findings and critical review or evaluation of new discoveries. The authors are required to confirm that their paper has not been submitted to any other journal in English or any other language.

ISOMAse

International Society of Ocean, Mechanical and Aerospace
-Scientists and Engineers-

Journal of Ocean, Mechanical and Aerospace
-Science and Engineering-
Vol.5: March 2014

Scope of JOMAse

The JOMAse welcomes manuscript submissions from academicians, scholars, and practitioners for possible publication from all over the world that meets the general criteria of significance and educational excellence. The scope of the journal is as follows:

- Environment and Safety
- Renewable Energy
- Naval Architecture and Offshore Engineering
- Computational and Experimental Mechanics
- Hydrodynamic and Aerodynamics
- Noise and Vibration
- Aeronautics and Satellite
- Engineering Materials and Corrosion
- Fluids Mechanics Engineering
- Stress and Structural Modeling
- Manufacturing and Industrial Engineering
- Robotics and Control
- Heat Transfer and Thermal
- Power Plant Engineering
- Risk and Reliability
- Case studies and Critical reviews

The International Society of Ocean, Mechanical and Aerospace –science and engineering is inviting you to submit your manuscript(s) to isomase.org@gmail.com for publication. Our objective is to inform authors of the decision on their manuscript(s) within 2 weeks of submission. Following acceptance, a paper will normally be published in the next online issue.

ISOMAse

International Society of Ocean, Mechanical and Aerospace
-Scientists and Engineers-

Journal of Ocean, Mechanical and Aerospace
-Science and Engineering-
Vol.5: March 2014

Editors

Chief-in-Editor
Jaswar Koto (Ocean and Aerospace Research Institute, Indonesia)

Associate Editors
Adhy Prayitno (Universitas Riau, Indonesia)
Agoes Priyanto (Universiti Teknologi Malaysia, Malaysia)
Ahmad Fitriadhy (Universiti Malaysia Terengganu, Malaysia)
Ahmad Zubaydi (Institut Teknologi Sepuluh Nopember, Indonesia)
Buana Ma'ruf (Badan Pengkajian dan Penerapan Teknologi, Indonesia)
Carlos Guedes Soares (Centre for Marine Technology and Engineering (CENTEC), University of Lisbon, Portugal)
Dani Harmanto (University of Derby, UK)
Iis Sopyan (International Islamic University Malaysia, Malaysia)
Jamasri (Universitas Gadjah Mada, Indonesia)
Mazlan Abdul Wahid (Universiti Teknologi Malaysia, Malaysia)
Mohamed Kotb (Alexandria University, Egypt)
Priyono Sutikno (Institut Teknologi Bandung, Indonesia)
Sergey Antonenko (Far Eastern Federal University, Russia)
Sunaryo (Universitas Indonesia, Indonesia)
Tay Cho Jui (National University of Singapore, Singapore)

Published in Indonesia.

JOMAse

ISOMAse,
Jalan Sisingamangaraja No.89
28282, Pekanbaru-Riau
INDONESIA
http://www.isomase.org/

Printed in Indonesia.

Teknik Mesin
Faultas Teknik
Universitas Riau, Indonesia

ISOMAse

International Society of Ocean, Mechanical and Aerospace
-Scientists and Engineers-

Journal of Ocean, Mechanical and Aerospace
-Science and Engineering-, Vol.5

March 20, 2014

Asymmetry Effect on Hydrodynamic Characteristics of Double Chamber Oscillating Water Column Device

Wilbert. R,[a,*], Sundar.V [b] and Sannasiraj.S.A [b]

[a)]*Assistant Professor, Civil Engineering Department, Govt.Engineering College Wayanad, Kerala, India-670644*
[b)]*Professor, Ocean Engineering Department, Indian Institute of Technology Madras, Chennai, India-600036*

*Corresponding author: wilbertcet@gmail.com

Paper History

Received: 10-February-2014
Received in revised form: 28-February-2014
Accepted: 10-March-2014

ABSTRACT

Awakening of renewable energy in the latter half of the twentieth century has identified wave energy as a potential source of clean energy due to its high intensity of energy flux compared with other renewable sources of energy. Subsequent research found out that Oscillating Water Column (OWC) concept is an easier and simple technology to harness energy from the Ocean waves. This had lead to a rapid progress in research pertaining to tuning of the system for optimum efficiency. The Double Chamber Oscillating Water Column (DCOWC) concept is a modified form of OWC. The present study is an extension of previous studies for understanding its hydrodynamics with respect to its two geometric parameters; bottom opening and front duct width. The experimental works carried out on a scaled down model for identifying the effective combination between them is explained. The hydrodynamic principles governing the maximum harness of wave energy is detailed here. The discussions related to wave energy absorption, wave energy conversion, phase angle difference between pressure excitation and air pressure and wave amplification which govern the efficiency of the DCOWC are included for a better understanding on the effect between geometry and wave characteristics. It is expected that the findings of this study enhance knowledge on the hydrodynamic aspects of the concept of a DCOWC.

KEY WORDS: *Wave Energy; Dynamic Pressure; Asymmetry; Phase Angle, Wave Amplification.*

NOMENCLATURE

b/B	Relative front duct width
C_A	Wave Power Absorption Efficiency
d/L	Relative water depth
E_{in}	Incident wave energy flux
λ	Energy conversion efficiency
η	Water surface elevation
Ψ	Cross correlation
β	Wave amplification
ϕ_d	Phase difference
ε_η	Spectral width parameter of the incident wave
ε_{p_f}	Spectral width of front wall pressure
ε_{p_r}	Spectral width of rear wall pressure
ε_{p_a}	Spectral width of air pressure
$[(m_0)_r]_{front}$	Dimensionless zeroth spectral moment of front wall pressure
$[(m_0)_r]_{rear}$	Dimensionless zeroth spectral moment of rear wall pressure
$[(m_0)_r]_{air}$	Dimensionless zeroth spectral moment of air pressure
$\frac{p_{f_{max}}}{\rho g H}$	Dimensionless front wall pressure
$\frac{p_{r_{max}}}{\rho g H}$	Dimensionless rear wall pressure
$\frac{p_{a_{max}}}{\rho g H}$	Dimensionless air pressure

1.0 INTRODUCTION

The ocean waves generated by the wind in the deep ocean propagate towards the coast and the energy being transmitted in its direction of propagation. The wave heights in the near shore that dictates the wave power potential may increase or decrease depending on the phenomena like shoaling, refraction, diffraction and their combined effects. The possibility of transporting mechanical energy available at one place in the form of electricity to other places made the energy extraction from ocean waves as a reality. Wave energy is an abundant, indigenous, renewable, clean and sustainable resource. Compared to other renewable energy sources, wave power has got energy density manifolds greater than that is present in wind and sunlight. Hence, there has been a significant and rapid increase in the research and developments in the field of extraction of energy from Ocean waves. Several concepts of the wave energy devices varying in shape and size have been tried through numerical, physical modeling as well as trial pilot plants in the open Ocean. In wave energy conversion process, initially the kinetic and potential energy forms of waves have to be converted into mechanical energy for rotating the turbines in order to generate electricity by means of an interface device. These devices are referred to as Wave Energy Converters (WECs). Wave energy research in a formal way has started with oil crisis of 1970's. Periods of research developed a variety of concepts for energy extraction and the details are given by Hagerman [1]. They are broadly classified into three categories; overtopping devices, wave activated bodies and Oscillating Water Columns (OWC). Among these, OWC has got the unique distinction of having turbine as the only moving component above the water surface. Hence operation and maintenance are easier in OWC device and thus, making it more attractive. Sundar et al.[2] have presented detailed view on socio-economic benefits achievable by integrating OWC with breakwaters. This can facilitate the sharing of costs involved in erecting a wave energy convertor as part of investment could be to protect an eroding coast which normally is exposed to converging of waves.

In its physical form an OWC device consists of a caisson having an opening towards the seaside. The dynamic pressure available at the interface between the structure and the water surface oscillates the water column inside the caisson to develop pneumatic power inside the air chamber. The heaving of water inside the caisson causes the cyclic air flow through a duct provided over the air chamber. By placing a biaxial turbine across the air flow, the bi-directional air flow is converted in to unidirectional rotation of the turbine for electricity generation. This concept was invented by Masuda of Japan [3] and initially it was applied in navigational buoys. To gain operational experience in converting low frequency wave system to match with the high frequency power grid, Masuda [4] conducted sea trial tests with a prototype floating OWC device. Later, the trend turned towards bottom mounted OWC devices, and with researchers focussing on methods of optimising the efficiency of the device and looking at economic viability in wave energy converters, that lead to integrating it with break waters as one of the options.

There have been continual studies of both experimental and theoretical to bring forth optimisation on energy conversion capacity of OWC devices. Ambili et al. [5] in physical model study found that a range of wave periods can cause oscillation inside the air chamber and introduced the Multi-resonant Oscillating Water Column (MOWC) concept. It was observed that provision of projecting side walls in front of the mouth opening improves the energy conversion capacity of the device. Count and Evans [6] studied the effect of projecting side wall by boundary integral method. Malmo and Reitan [7] numerically studied the effect of geometry, wave frequency and direction on energy conversion capacity of OWC devices set in reflecting walls. McIver and Evans [8] adopted the method of matched asymptotic expansion for solving the hydrodynamics of OWC devices. Zheng [9] conducted physical model studies for parametric optimisation and reported that flared harbour walls are more effective for energy conversion rather than rectangular ones. Evans and Porter [10] studied the effect of chamber width, perpendicular to the wave crest, effect of lip wall submergence on energy conversion capacity of the device through theoretical investigations. It was observed that as the depth of submergence increased, the energy conversion from low period waves decreased significantly. It shows that an increase in the submergence depth increases the natural period of the device. Ma [11] through laboratory models formulated analytical expression for natural period of the OWC devices. It was found out that the natural period is inversely proportional to the bottom opening depth. Thus, it is made clear that OWC principle is analogous to forced vibration problem, wherein, the response is determined by both the magnitude and frequency of exciting force. Larger opening of OWC as the bottom is found to be more effective in absorbing higher frequency waves, whereas, lesser opening is found to be more effective in absorbing low frequency waves. To solve the problem of frequency effect between device and the excitation force, studies have been conducted to tune the natural frequency of the device by adjusting the damping level to the hydrodynamic efficiency with respect to frequency. Korde [12] concluded that reactive control of wave energy devices works well for absorbing energy from longer period waves.

Boccotti [13] proposed a modified concept of OWC by incorporating a duct in front of the bottom opening. The intension is to capture the maximum intensity of dynamic pressure for oscillation inside the air chamber. Through analytical studies, it was found that the power absorption capacity of the device at the mouth can reach up to 100%. Later through a field study, Boccotti et al. [14] confirmed the theoretical predictions agree with the experimental observations. It was also observed, that the front duct increases the natural period of the device which can absorb energy from long waves. In its physical form, this device consists of two chambers for the water flow in energy conversion process, hence it is called as the Double Chamber Oscillating Water Column (DCOWC). Since DCOWC device operates like a dynamic system and is under the influence of radiation damping and added mass in wave structure interaction, it is very essential to know the influence of front duct on its hydrodynamic performance. In the present work, this aspect has been studied by changing the front duct width relative to width of energy conversion chamber.

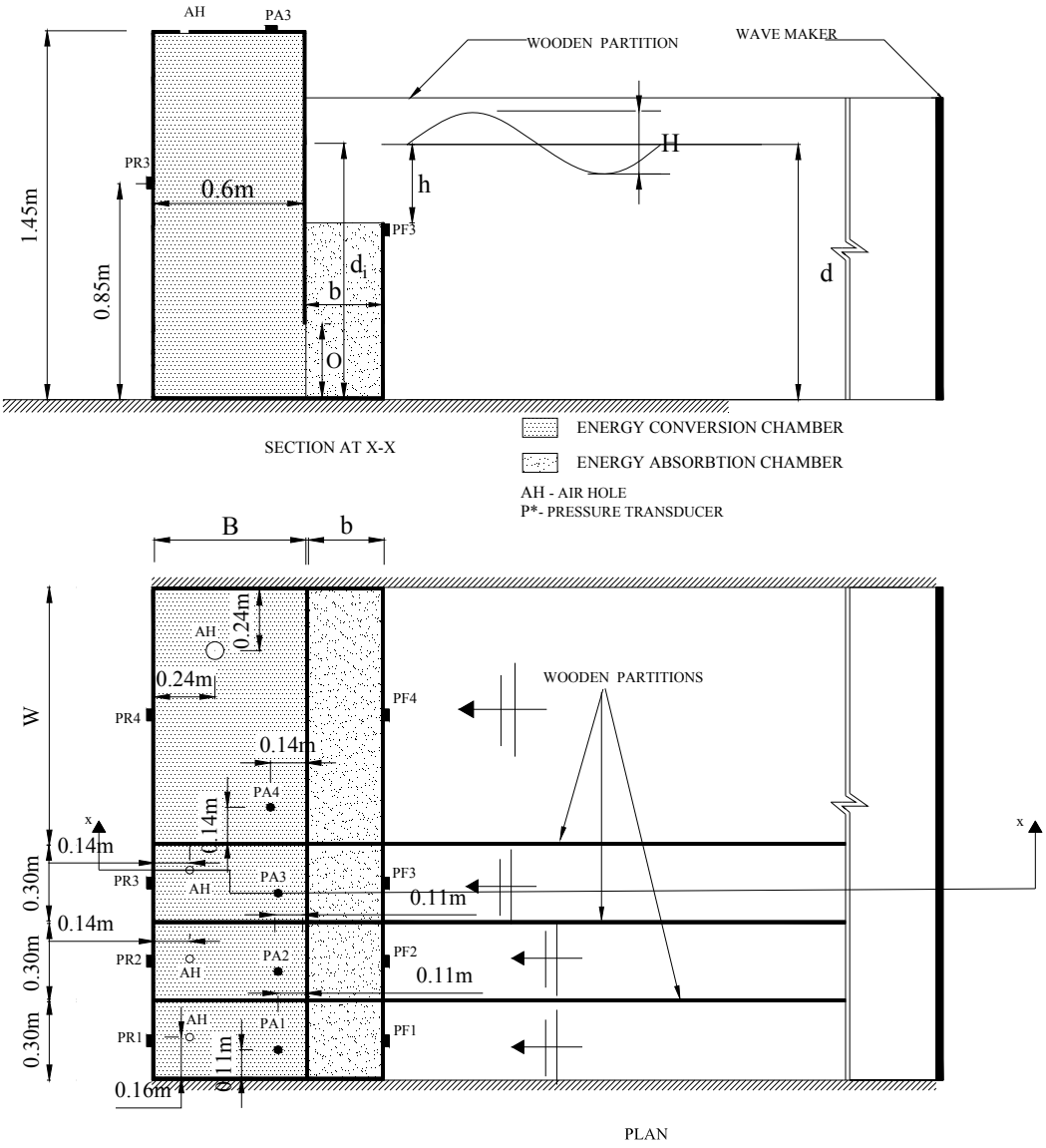

Figure 1: Plan and section of the model.

2.0 EXPERIMENTAL SET UP

The experiments were carried out in the wave flume of 72.5m long, 2m wide and 2.7m deep at the Department of Ocean Engineering, Indian Institute of Technology, IIT Madras, India. The physical model consists of four DCOWC model units integrated together. This facilitated simultaneous testing of models of different system parameters to particular wave characteristics. Considering the dominance of gravity force in wave structure interaction problem, Froude similitude criteria is adopted and a model scale of 1:20 was assigned in accordance with the guide lines of Sarmento and Thomas [15]. Each device has two parts namely the front chamber, the energy absorption chamber and the rear chamber, the energy conversion chamber. Among the four DCOWC units, three are smaller of same size having energy conversion chamber of 0.30mx0.6mx1.45m and the fourth is of 1.00mx0.60mx1.45m. The energy absorption units of fiber reinforced plastic covered over steel frame had a depth of 0.70m and the width(W) parallel to the wave crest was kept same as the width of the respective energy conversion unit and the width (b) perpendicular to the wave crest varied as 0.15m, 0.30mand 0.45m. To change the width, provisions were made in the frame work to fix the vertical plate at the respective locations. The top of the energy conversion chambers were covered with 12mm thick perpex sheets to view the nature of water oscillations inside the air chamber. To achieve water and air tightness at joints silica gel was used. For simulating the turbine effect on energy conversion chambers, circular air holes having 0.65% of its plan

area were provided. Wang et al. [16] have reported OWC experimental works carried out with similar provisions for damping. Thiruvenkatasamy and Neelamani [17] have reported a decrease in the efficiency for air hole area beyond 0.85%. Rapaka [18] through model studies concluded that the energy conversion processes is optimum for the air hole area within a range of 0.45% to 0.68% of water plane area.

The plan and sectional view of the model adopted for the present study is shown in Fig.1 The model parameters that are likely to govern the efficiency of the device considered are bottom opening depth (O), width (W) parallel to the wave crest, width (B) perpendicular to the wave crest and the width (b) of the energy absorption chamber. The depth (h) for mouth opening was set to 0.30m and maintained constant throughout the tests. The bottom opening depth, for the smaller units were 0.15m, 0.30m and 0.45m, whereas, for the larger unit, it was 0.30m. The depth (d) of water in the flume was kept at 1.0m. The depth (d_i) water inside the model was same as d. The width of the energy conversion chamber of the caisson, 'B' for the energy conversion unit was 0.60m, whereas, for energy absorption unit 'b' was varied in terms of 0.15m, 0.30m and 0.45m . The width 'W' for the bigger and smaller units was 1.0m and 0.30m respectively. To avoid any possible interference effect, the adjacent units were separated by plywood partitioning for a length of 11m along the flume. Wave gauges of conductivity type measured the time histories of water surface elevation and the pressure sensors having maximum range of 0.2bar and 0.5bar were used for measuring the air and water pressures respectively. The locations of these measurements are indicated in the above figure. The photographic view of the model with the accessories is shown in Fig.2. The model units were exposed to the action of both regular waves of periods, T ranging between 1.2s and 2.4s at an interval of 0.1s. and random waves. For each period, wave heights of 0.045m, 0.055m, 0.065 and 0.045m were employed. In addition, tests with random waves following Pierson-Moskowitz (PM) spectrum were also considered for the tests, in which case, the peak period, T_P was varied from 1.2s to 2s at an interval of 0.2s. For each T_P three significant wave heights, H_S of 0.055m, 0.065m and 0.095m were adopted for the tests.

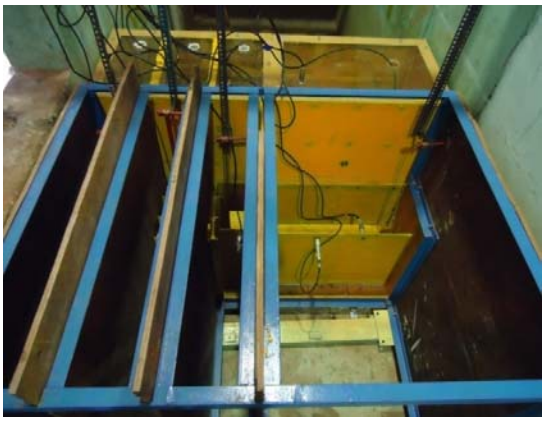

Figure 2: A view of the model.

For studying the effect of asymmetry between the energy absorption chamber and the energy conversion chamber, three test cases for b/B = 0.25, 0.50 and 0.75 were taken up. Considering the system parameters combination and wave characteristics, a total number of 201 test runs were executed for data collection.

3.0 RESULTS AND DISCUSSION

Typical time series of measured quantities, wave elevation, η, pressure on the front wall, p_f, pressure on the rear wall, p_r and air pressure, p_a, for a wave of H= 0.095m and T=2.3s for the model with b/B=0.25 and O/d_i=0.45 are shown in Fig.3 The velocity of water oscillation inside the energy conversion chamber is obtained through numerical differentiation of rear wall pressure and air pressure. Central difference scheme was adopted to reduce the order of error in the computation. While, analysing data the under regular waves, three successive steady cycles after the transient state were considered. To study the effect of water plane area on pneumatic damping, energy conversion efficiencies, results for two W/B of 0.5 and 1.67 were considered. Since the efficiency values for the two units were nearly same, the results of smaller units are reported herein.

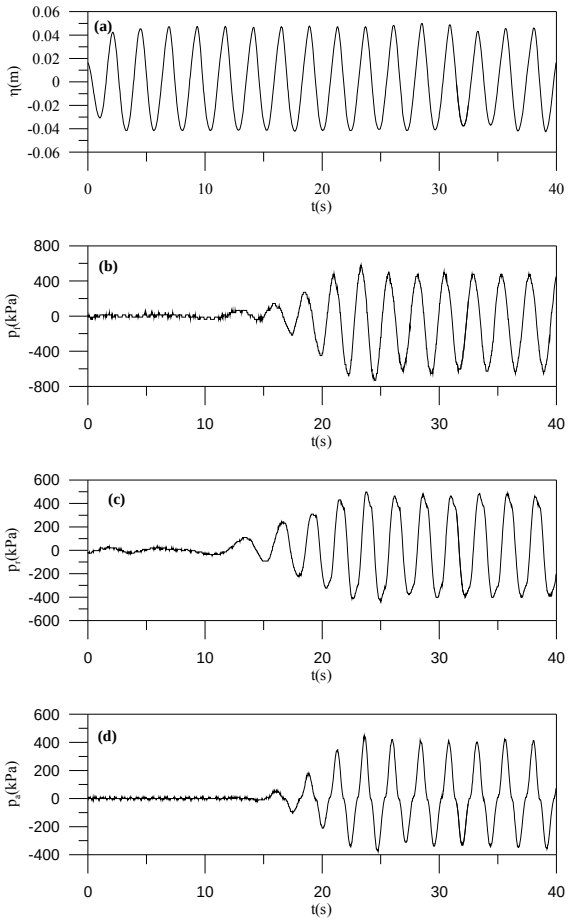

Figure 3: Time history of (a) incident wave surface elevation, (b) front wall pressure, (c) rear wall pressure and (d) air pressure.

3.1 Wave power absorption

For a DCOWC exposed to the waves, the dynamic pressure beneath the wave induces the necessary driving force at its mouth that is responsible for the water surface oscillation inside the energy conversion chamber. This causes water flow over the mouth in the vertical direction. Boccotti [13] computed the wave power absorption efficiency (C_A) at the mouth in terms of the velocity of flow(v_m), the dynamic pressure (p_f) , plan area (A_m) of mouth, width (W) and the incident wave energy flux (E_{in}) as detailed in Eqn. (1).

$$C_A = \frac{\frac{1}{T}\int_{t}^{t+T} p_m v_m A_m dt}{E_{in}} \quad (1)$$

The energy flux (E_{in}) across the width (W) associated with the given wave height (H), period (T) propagating with celerity (C) in water depth (d) across the width (W) is computed following linear wave theory and is as per Eqn. (2).

$$E_{in} = \frac{\rho g H^2}{8} \cdot \frac{C}{2}\left(\frac{2kd}{\sinh 2kd} + 1\right) W \quad (2)$$

where, $k = \frac{2\pi}{L}$, L is the wave length

The influence of b/B and O/d_i on the variation of wave power efficiency, C_A against the relative water depth, 'd/L' for a constant wave height of 0.095m for O/d_i=0.15, 0.30 and 0.45 are presented in Figs. 4a-c respectively. The results show that for the three O/d_i, the C_A decreases with an increase in d/L and is found to be a maximum for the longest wave tested and decreases as the waves become shorter. This is probably due to the reflection of longer waves from any obstruction being more leading to amplification of the waves near the opening into the chamber of the device. Further, the C_A is found to increase with an increase in the O/di as larger power is expected to propagate into the energy conversion chamber, which is found to be pronounced for d/L less than 0.25. The results also demonstrate that the wave power efficiency of the DCOWC is higher in relatively shallower waters. The effect of b/B is least for the smallest O/d_i of 0.15 tested. Since the physics of C_A follows linear circuit theory [19] there exists the possibility of entire mouth pressure not being fully utilised for causing flow inside the energy conversion chamber. In wave structure interaction the mouth pressure splits into two components namely active part and reactive part. The active part contributes to the velocity of flow and reactive part contribute to the wave height growth in front of the structure. Hence it is difficult to conclude the hydrodynamic effectiveness of the device under varying b/B based on C_A.

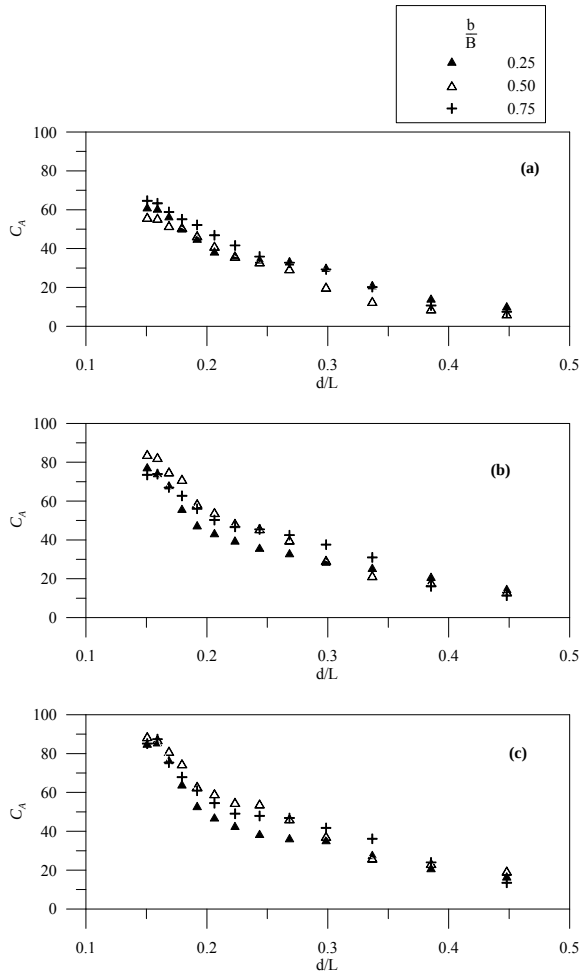

Figure 4: Effect of asymmetry on wave power absorption efficiency at (a) O/d_i=0.15, (b) O/d_i=0.30 and (c) O/d_i=0.45

The effect of wave steepness on C_A, as a function of d/L for the three b/B for the structure with O/d_i=0.45 and h/d_i =0.30 for b/B=0.25, 0.50 and 0.75 are brought out in **Figs. 5a-c** respectively. The effect of H/L is observed to be the least for the least b/B of 0.25 tested, whereas, it is found to be more pronounced for the other two indicating certain degree of nonlinearity either in velocity of flow or on pressure developed at the mouth. The C_A is found to reach 100% for d/L about 0.1 which agrees with the findings of Boccotti et al. (2007).. The trends observed over the wave power efficiency variation necessitate further analysis for ascertaining the best combination of b/B and O/d_i for maximum possible energy.

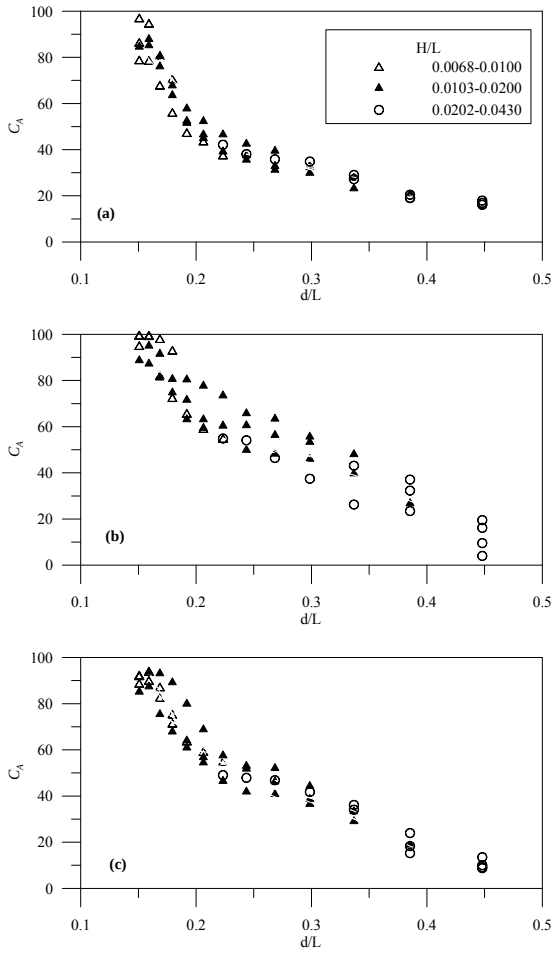

Figure 5: Effect of wave steepness on wave power absorption efficiency at O/d_i=0.45 for asymmetry values of (a) b/B=0.25, (b) b/B=0.50 and (c) b/B=0.75

3.2 Energy conversion efficiency

DCOWC converts wave energy in to pneumatic energy which rotates the turbine for electricity generation. Since pneumatic power calculation is very difficult due to the measurement of both velocity and pressure at the air hole, researchers compute [16, 17, 20, 21] the hydrodynamic power using the velocity of water surface oscillation and air pressure. In agreement with the existing methodology, the energy conversion efficiency (λ) is computed from hydrodynamic power developed and incident wave power as per Eqn. (3)

$$\lambda = \frac{\frac{1}{T}\int_{t}^{t+T} p_a A v dt}{E_{in}} \times 100 \qquad (3)$$

where p_a is the air pressure, v is the velocity of water surface oscillation inside the air chamber, A is the plan area of air chamber and E_{in} is the incident wave power computed as per Eqn. (2). The effect of O/d_i on the variation of λ with d/L for the three b/B's for a constant wave height of 0.095m is brought out in Figs. 6a-c. Herein, h/d_i is mainatained as 0.30. The variation of B/L is also incorporated in the plot.

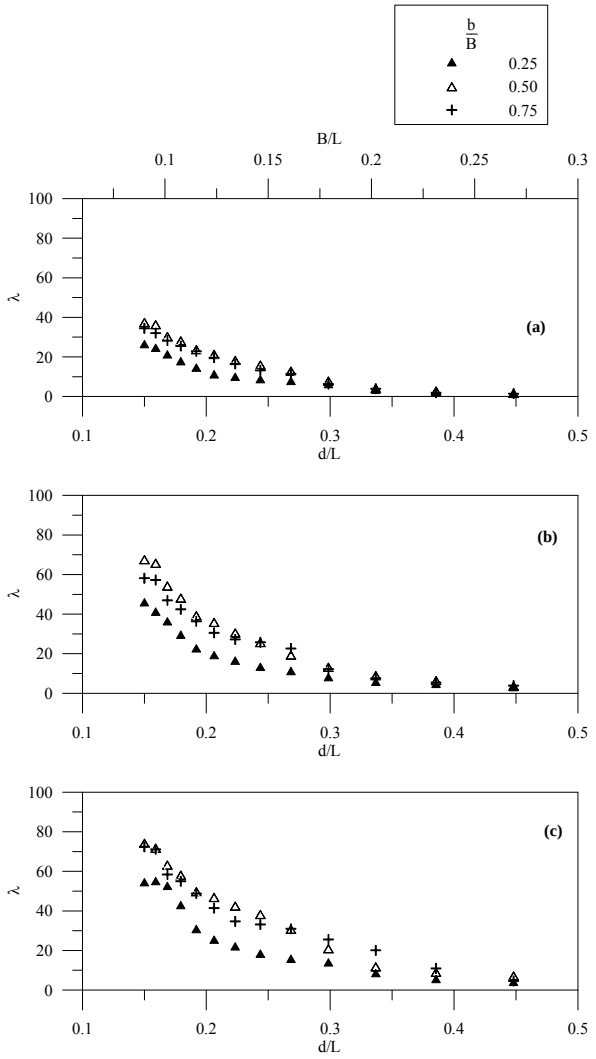

Figure 6: Effect of asymmetry on energy conversion efficiency at (a) O/d_i=0.15, (b) O/d_i=0.30 and (c) O/d_i=0.45

The effect of asymmetry in hydrodynamic performance is explicitly revealed in these figures. The low efficiency associated with the lowest b/B can be considered as the characteristic feature of DCOWC. The slope of the trend line for b/B=0.25 (Fig. 6c) up to d/L of 0.2 indicates the zone closer to the resonance region and the system exhibits an orientation towards energy conversion. However, the steady value of λ for the lowest frequency indicates that wave reflection is dominating at the mouth of the device. This can be explained by considering the higher values for group celerity at lower frequencies. As the wave moves past the vertical wall of front duct, it feels the obstruction like a submerged wall and gets partially reflected. Further, the lower values of λ at b/B =0.25 indicates the predominance of energy reflection rather than

energy absorption. In wave structure interaction, the growth of added mass with respect to the geometry of the device may be the reasons for the lower performance in energy conversion. The increase in λ with an increase in O/d_i below d/L=0.20 and B/L=0.125 may be due decrease in the flow length and corresponding changes in the natural period of the systems. The loss due to wall friction is not considered herein. The convexity over the trend line of λ at lower values of d/L for O/d_i=0.45 at b/B=0.25 may be due to the higher wave celerity, the waves moving past the vertical plate of the front duct feels the vertical face of air chamber and gets reflected. The absence of this trend for O/d_i=0.15 and 0.30 can be related to the natural period variation. The comparison of λ for b/B of 0.50 and 0.75 indicates that the variation is marginal. A slight decrease in λ for b/B=0.75 compared to that for b/B=0.50 indicates that for b/B>0.75, the dynamic pressure excitation is likely to undergo modulation. Thus, the comparative analysis conclusively prove that the system performs well with a characteristic asymmetry with b/B=0.50.

Since the energy conversion assumes forced vibration behaviour, as the natural period changes corresponding changes are induced over the phase angle difference between air pressure and dynamic pressure excitation. The fundamental principle behind the energy conversion can be related to the theory of linear circuit where the output power is in direct proportion with the cosine function of phase angle. From the asymmetry effects it is observed that better performance is for the system with b/B=0.50 and O/d_i=0.45. The important aspect in DCOWC is that the dynamic pressure below the wave behaves as the forcing function at the mouth opening of front duct. Herein, as the asymmetry increases there is a possibility for the wave interaction phenomena to become a wave transmission type where the hydrodynamics gets adversely modified. This is revealed in the figure as the λ values at b/B=0.75 takes lower values compared to its counterparts at b/B=0.50. The trend line of λ at b/B=0.75 for d/L> 0.30 coming above the trend line of lower asymmetry values may be due to the discharge effect under the waves.This follows the control effect of harbour wall in Single Chamber Oscillating Water Column (OWC) as observed by Ambili et al.[5]. Thus, for h/d_i=0.30, the asymmetry value b/B=0.50 exhibits a better efficiency in its performance. It is understood that for an efficient performance in pneumatic power conversion, the water surface inside the energy conversion unit has to follow piston mode movement. The recent study of on OWC by Zhang et al. [21] showed that there are possibilities for sloshing mode behaviour in water oscillation depending on device width perpendicular to wave crest. With this as the background, in the present study it is observed that the maximum efficiency to an extent of about 80% occurs for B/L around 0.10. Further analysis is required to also consider the effect of variation with phase angle prior to concluding the magnitude of B/L.

The effect of wave steepness on the variation λ with d/L for O/d_i = 0.45 for the three b/B are plotted on Figs.7a-c.For all the b/B tested, it is seen that λ decreases with an increase in d/L. The insignificant effect of H/L on λ for b/B=0.25, indicates predominance of wave reflection at this asymmetry value. This substantiates the increase in added mass effect, the flow has to negotiate in causing oscillation inside the air chamber.

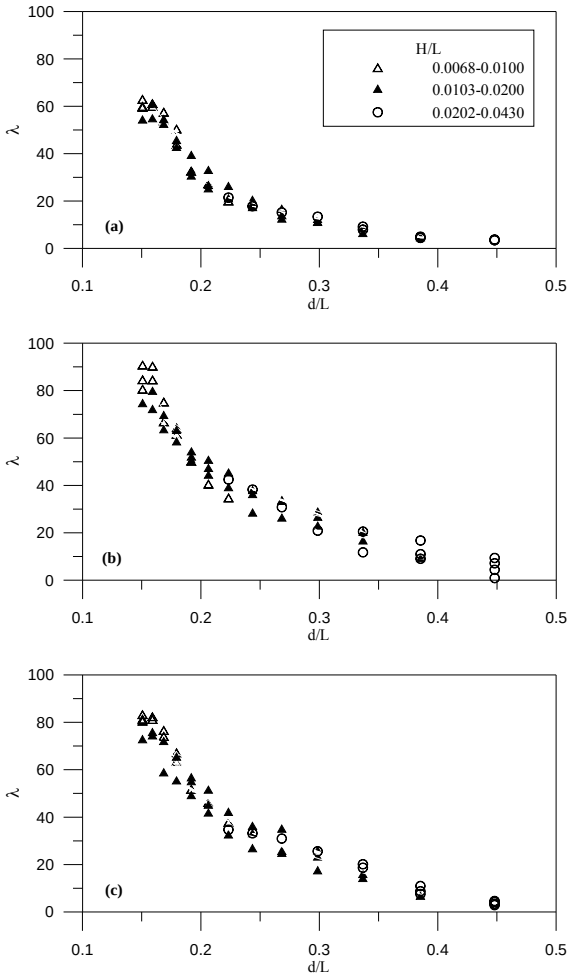

Figure 7: Effect of wave steepness on energy conversion efficiency at O/d_i=0.45 for asymmetry values of (a) b/B=0.25, (b) b/B=0.50 and (c) b/B=0.75.

The effect of H/L (for H/L ranging between 0.0068 and 0.043) for a particular d/L is found to be insignificant. λ is found to decrease with an increase in d/L and for the lowest d/L it attains a maximum of about 60%. It is clear that λ is inversely proportional to the wave frequency. It is further observed for b/B=0.75 that λ for lower d/L is about 70%. For the small wave steepness, an increase in λ up to about 10% is noticed. This indicates that as H/L increases, the energy loss associated with the fluid flow is more.

3.3 Phase angle variation

The basic preposition behind the working of DCOWC is the increase in both natural period of the system and the dynamic pressure available for oscillation. In OWC, the natural period of the system can be increased by decreasing the opening depth which causes a reduction in dynamic pressure available for forcing. As the bottom opening increases, there are possibilities for wave trough clearing the lip wall depth and air enters through the front mouth opening causing stalling for the turbine and

power shut down in the system. This limitation of OWC is thus overcome in DCOWC by providing front duct. The variation of phase angle (ϕ_d) as computed

$$\phi_d = 360 \times \frac{T^*}{T} \tag{4}$$

where, $\Psi\ (T^*)$ is the lag of the absolute maximum of cross-correlation between wave pressure (p_f) at the mouth and the air pressure (p_a) inside the air chamber.

$$\Psi\ (T^*) = \langle p_f\ (t)\ p_a\ (t + T^*) \rangle \tag{5}$$

The variation of phase angle between dynamic pressure excitation and air pressure for b/B = 0.25, 0.50 and 0.75 for O/d_i = 0.15, 0.30 and 0.45 are plotted in Figs.8a, b and c respectively.

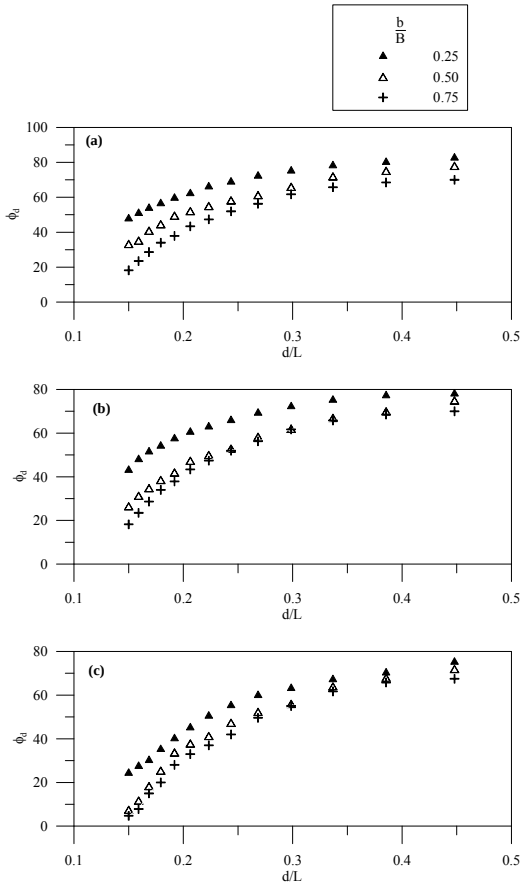

Figure 8: Effect of asymmetry on phase angle variation at (a) O/d_i=0.15, (b) O/d_i=0.30 and (c) O/d_i=0.45

It is observed that ϕ_d for b/B=0.25 is exceptionally high. This is probably due to the longer stream line length in the flow occurring inside the DCOWC. The possible reasons for this phenomenon are the added mass effect and the wave amplification occurring near the mouth of the device. The reason for the regressive performance in energy conversion efficiency for b/B of 0.25 is attributed to larger phase variation. For d/L >0.25, ϕ_d for b/B= 0.50 and 0.75 reaches an asymptotic value indicating an out of phase condition. It is inferred that the DCOWC response to higher frequencies is low. It can be substantiated by observing the corresponding energy efficiency values. A diminishing trend for O/d_i=0.30 and 0.45 are observed (Figs. 8 b and c). Similarly, for d/L < 0.25, there exists slight variation over ϕ_d for O/d_i=0.15. It shows that the added mass effect and the wave amplification are negligible over the above frequency range for these system parameters.

The phase variation due to the asymmetry in the device, thus, indicates that the geometrical system parameters can be tuned by understanding the phase difference. The phase variation and corresponding energy conversion efficiency indicate that phase difference is the central aspect in the design of DCOWC device. For maximum energy conversion, the phase difference between the wave and the fluctuating air column should be close to zero. This can be realized by suitably selecting the system parameters to bring the natural frequency of the system closer to the predominant wave frequency.

3.4 Wave amplification

The assessment of energy conversion process is the primary criteria for the evaluation of the DCOWC concept. A qualitative evaluation of the relationship between different device parameters in regulating the conservation principles is an important aspect to formulate design criteria. The wave height growth in front of the structure is called as the wave amplification (β) and it is computed as

$$\beta = \frac{H_m}{H_{in}} \tag{6}$$

where, H_m is the wave height in front of the device and H_{in} is the incident wave height..

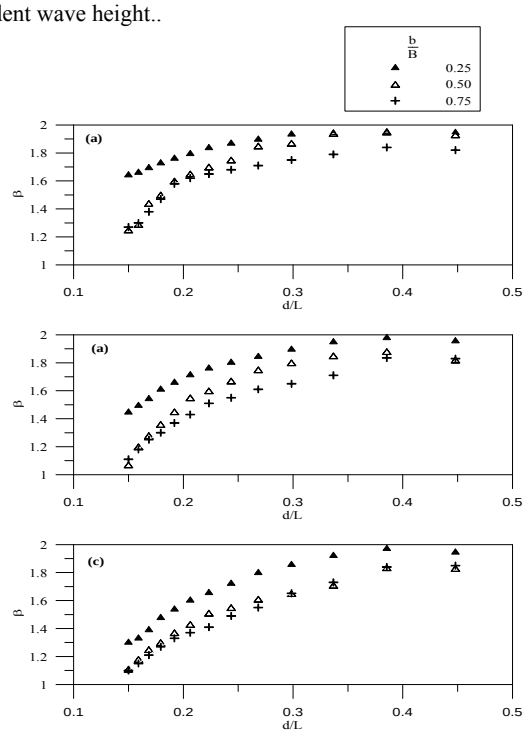

Figure 9: Effect of asymmetry on wave amplification at (a) O/d_i=0.15, (b) O/d_i=0.30 and (c) O/d_i=0.4.

The degree of variation of β for the three asymmetry factors is presented for O/d_i =0.15, 0.30 and 0.45 in Figs.9a, b and c, respectively It is evident that, in general, β increases with d/L. This indicates that the system is tending towards the resonance region with a decrease in the frequency of excitation. The reason for the lesser energy conversion for b/B=0.25 can be inferred from the trend in their variation. It is observed that irrespective of the relative bottom opening $O/d_{i,}$, β takes relatively larger values for DCOWC with b/B=0.25. At low asymmetry factor, the waves get amplified near the mouth constraining the flow in to the device. The possible reason for this phenomenon can be related to the added mass effect developing in the present wave structure interaction problem. This agrees with the general concept existing for the added mass that it depends mainly on the structural configuration.

Furthermore, for d/L < 0.20, β takes closer values for b/B=0.50 and 0.75, which shows that the mouth captures the incoming energy and β is higher for the least asymmetry at the lowest frequency indicating the minimum capture of energy at the mouth. For d/L > 0.30 , it is observed that the trend lines of β for O/d_i=0.15 at b/B=0.25 and 0.50 merge, while, the same for b/B=0.75 is less. It is an indication that larger asymmetry factor modulates the wave profile. That is, beyond a critical b/B, the wave interaction can transform into a wave transmission problem making the regime of performance entirely different from what is envisaged as a DCOWC.

3.5 Pressures

To investigate the asymmetry effect in a boarder sense, its effect on the wave induced pressures on the front and rear walls as well as on the air pressures are plotted for a constant wave height of 0.095m in Figs.10, 11 and 12 respectively. The peak pressures are plotted in non dimensional form after normalising it with wave height as a function of d/L. In each of the above figures, the variations of the pressures for the three O/di tested are superposed for b/B=0.25,05 and 0.75. The results show that the pressures on the front wall decreases as d/L decreases and the rate of decrease being more drastic uto d/L of 0.3, beyond which, the effect is not significant. The peak pressure is a maximum at the lowest d/L tested for all the test conditions. The results also show that the wall with the largest O/di of 0.45 experiences least pressure for all d/L and b/B. Furthermore, The model with the least b/B of 0.25 is found to experience more pressures compared to the other two larger b/B of 05 and 0.75. This may be due to multiple reflection between the front wall and the energy conversion chamber, which is likely to reduce as the gap between increases. This indicates that the asymmetry effect beyond a critical limit will modulate wave forcing over the mouth. For a DCOWC, the combination of b/B=0.50 and O/d_i=0.45, rear wall pressure and air pressure at the lowest d/L reaching nearly equal to front wall pressure indicate that the system performance is better at the resonance region.

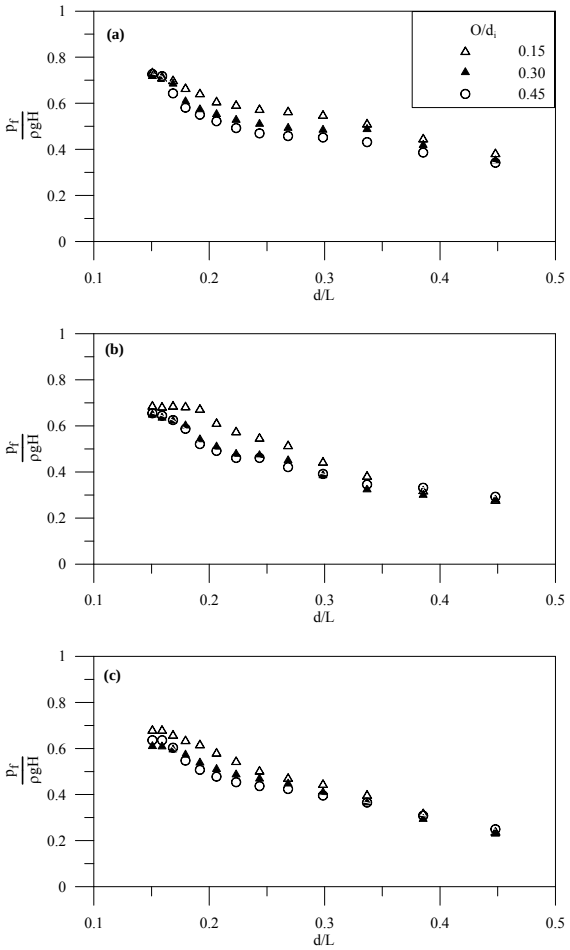

Figure 10: Effect of asymmetry on front wall pressure at (a) b/B=0.25, (b) b/B=0.50 and (c) b/B=0.75

Table 1: Comparison between energy conversion under regular and random waves (b/B=0.75, O/d=0.45).

$(d/L)/(d/L_P)$	Energy conversion Under regular waves	Energy conversion under irregular waves	Percentage change in Energy conversion
0.448	4.61	6.67	+44.69
0.3368	20.11	15.44	-23.22
0.2683	30.96	26.10	-15.70
0.2233	34.70	31.96	-7.90
0.1919	48.80	45.34	-7.09

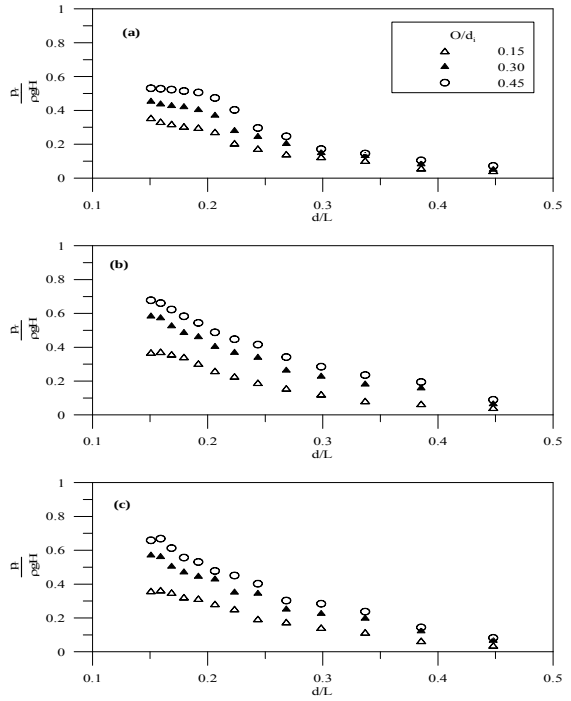

Figure 11: Effect of asymmetry on rear wall at (a) b/B=0.25, (b) b/B=0.50 and (c) b/B=0.75.

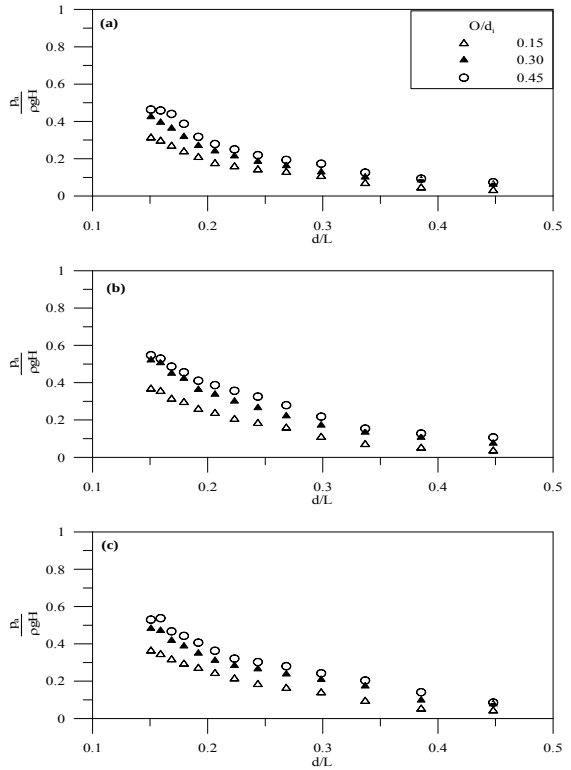

Figure 12: Effect of asymmetry on air pressure at (a) b/B=0.25, (b) b/B=0.50 and (c) b/B=0.75.

3.6 Random wave

The real sea state is random in nature. It is a prerequisite to assess the hydrodynamic characteristics by simulating similar sea state in the laboratory. By studying the interaction with random waves, the asymmetry effect of the device as compared to the same under regular waves can be brought out. The random waves defined by Pierson–Moskowitz (PM) spectrum were adopted for the tests. The characteristic factors of the spectrum are significant wave height (H_s) and peak wave period (T_p). Under the random wave incidence, the air pressure and the velocity of free surface are also of random in nature. Thus, the device has to be designed for average power development. The average power (P_{ave}) is calculated from significant velocity of free water surface oscillation (v_0) and significant air pressure (p_0) following the general methodology as,

$$P_{ave} = \frac{1}{2} p_0 A v_0 \tag{7}$$

wherein, A is the cross sectional area of the oscillation chamber. The incident energy flux (P_{in}) is calculated using significant wave height and group celerity (C_g) corresponding to peak wave period as,

$$P_{in} = \frac{1}{8} \rho g H_S^2 C_g \tag{8}$$

The energy conversion capacity (λ_R) is determined as

$$\lambda_R = \frac{P_{ave}}{P_{in}} \times 100\ \% \tag{9}$$

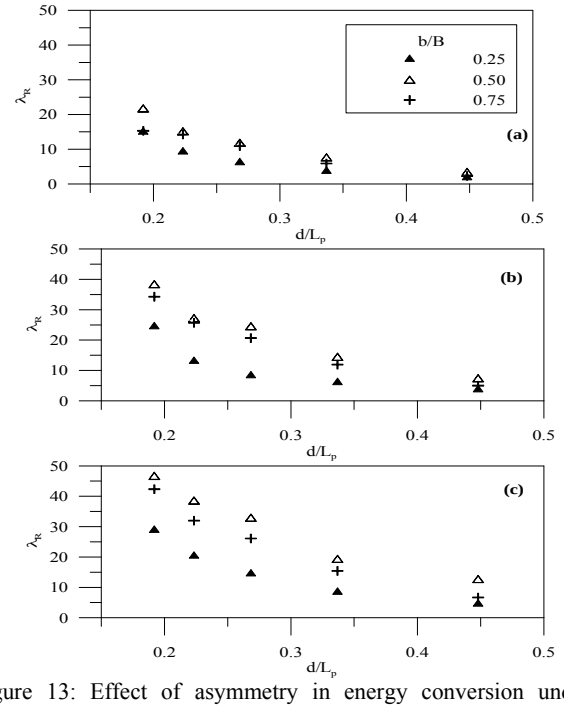

Figure 13: Effect of asymmetry in energy conversion under random waves (a) O/d_i =0.15, O/d_i =0.30 and (c) O/di =0.45.

The variation of energy conversion capacity (λ_R) with the relative water depth (d/L_P) for three b/B's aganist O/d_i=0.15, 0.30 and 0.45 are presented in Figs. 13 a, b and c, respectively. The

wave height here is H_S=.095m. λ_R achieves relatively higher values at b/B=0.50 under each O/d_i. The trend observed indicate that energy conversion under random waves depends mainly on device configuration and peak wave period. Table 1 summarises the energy conversion under both regular and random waves. The percentage changes were calculated taking energy conversion under regular wave as the reference value. This table illustrates that the device is towards resonance condition with the increase in peak period of the incident wave.

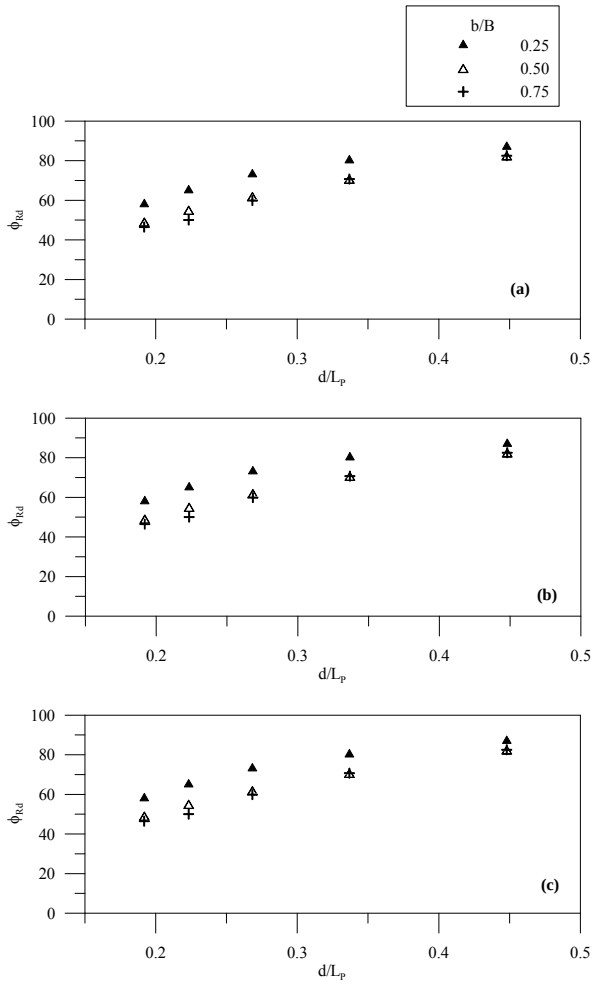

Figure 14: Effect of asymmetry in phase difference under random waves (a) O/d_i =0.15, O/d_i =0.30 and (c) O/di =0.45.

Further analysis over the sensitiveness of device with respect to peak wave period carried out under the phase difference (ϕ_{Rd}) between air pressure and incident dynamic pressure are plotted in Figs.14 a, b and c. The results do demonstrate an increase in natural period for the lower asymmetry at b/B=0.25. The explanation was given in section 3.3 holds true here also. The exact reasoning behind the increase in energy conversion with peak wave period can be inferred from the lower values of phase difference. These results substantiate that tuned system of DCOWC can hydrodynamicaly convert energy from random waves without any limitations. To have clear understanding on random wave structure interaction, the effect asymmetry plays on wave amplification (β_R) over the mouth is investigated. β_R is computed between maximum incident wave height (H_{maxi}) and maximum wave height at mouth (H_{maxm}) as per

$$\beta_R = \frac{H_{\max m}}{H_{\max i}} \tag{10}$$

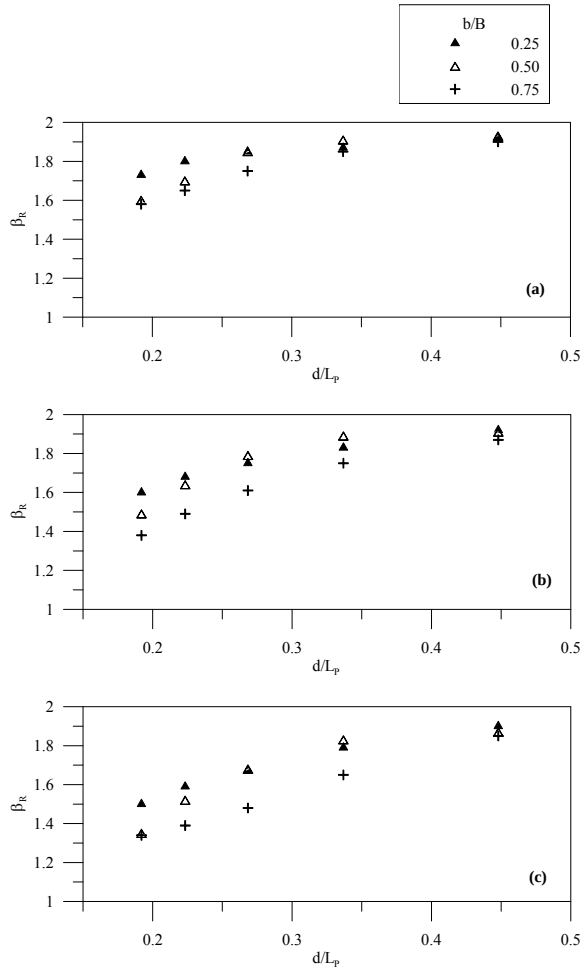

Figure 15: Effect of asymmetry in wave amplification under random waves (a) O/d_i =0.15, O/d_i =0.30 and (c) O/di =0.45.

β_R plotted for the three asymmetry values against the frequency parameter d/L_P are presented in Figs.15a-c. The trend follows the similar pattern observed under regular waves for the same. This shows that for tuned system, the maximum wave height present under random waves does not contribute to wave height growth near the device. To describe the asymmetry effect adequately tests carried out under the regime of random wave conditions are analysed in the subsequent sections.

3.7. Spectral width

In section 3.3 it was observed that asymmetry along with relative bottom opening produces phase control effect on energy absorption. Hence, studies on the effect of phase control over the spectral width of front wall, rear wall and air pressures are required for identifying the optimum combination of system parameters. The spectral width of the incident wave elevation, ε_η used at asymmetry values 0.25, 0.50 and 0.75 are presented in Figs.16a, b and c respectively. The figure indicates that all the waves used in the study had spectral width around 0.50. The effect of asymmetry over front wall pressures is plotted in Figs 17a-c. It is evident that at O/d_i=0.15, the spectral width 'ε_{p_f}' for front wall remains around 0.40 irrespective of b/B. This may be due to the effect of more reflection from the device. The spectral width value reaching more than 0.5 for higher values of d/L_p at b/B=0.25 and O/d_i=0.30 indicates that incoming wave splits in to higher order components after hitting front wall of energy conversion chamber. The lack of spread and change in the trend line for the spectral width at b/B=0.50 indicates that this asymmetry does not modulate the incoming wave. The trend line change for b/B=0.75 at O/d_i's 0.30 and 0.45 show the asymmetry effect interference with the incoming wave.

The effect of b/B's and O/d_i's combination on rear wall pressure under the varying wave conditions are plotted in Figs. 18a-c. These figures illustrate the phase control effect in a clear manner. The rear pressure represents the water oscillation characteristics inside the energy conversion units. It is to be seen that larger spectral widths are indication of poor performance while smaller spectral widths are for the energy concentration around the peak period. For the better performance the latter aspect is a desirable thing in the design. The larger values of ε_{p_a} at b/B=0.25 indicate the underperformance of the device at this asymmetry value. From this, it can be inferred that the stabilised value for ε_{p_r} reaches around 0.40 at b/B=0.50 and O/d_i=0.45. This is agreeable with respect to the incident wave having spectral width of 0.50. The spectral width parameter reaching to the above value for the least favourable system parameters combination (b/B=0.25 and O/d_i=0.30 and 0.45) at the highest d/L_P tested indicates that by suitable combination of system parameters with respect to the incident wave characteristics, tuning effect can be produced in the device for maximum energy conversion.

The air pressure spectral width 'ε_{p_a}' variation against d/L_p for the system parameters b/B and O/d_i are plotted in Figs.19a-c. The spectral width varies within a range of 1.0-0.50 with increase in d/L_p. The larger values at b/B=0.25 for O/d_i's 0.15, 0.30 and 0.45 are due to the greater phase variation within the device for the system parameters combination. In general it is observed that there is decrease in spectral width with increase in peak period. Among the configurations tested, the best system parameters identified are b/B's 0.50 and 0.75 at O/d_i's 0.30 and 0.45.

3.7 Spectral energy ratio

To study the device response under different system parameters and wave characteristics, ratio between spectral energies of front wall pressure, rear wall pressure and air pressure to the corresponding incident wave energy represented as $[(m_0)_r]$front, $[(m_0)_r]$rear and $[(m_0)_r]$air are shown in Figs.20,21 and 22 respectively. In Fig.20, observed that at a particular b/B, the energy ratios are getting relatively higher values with decrease in O/d_i. The high values around 1.2 are reached at O/d_i=0.15. The same for the largest asymmetry b/B=0.75 reaches around one. This indicates that energy reflection is more at O/d_i=0.15. In the same manner it is observed that energy absorption is more at O/d_i=0.45.

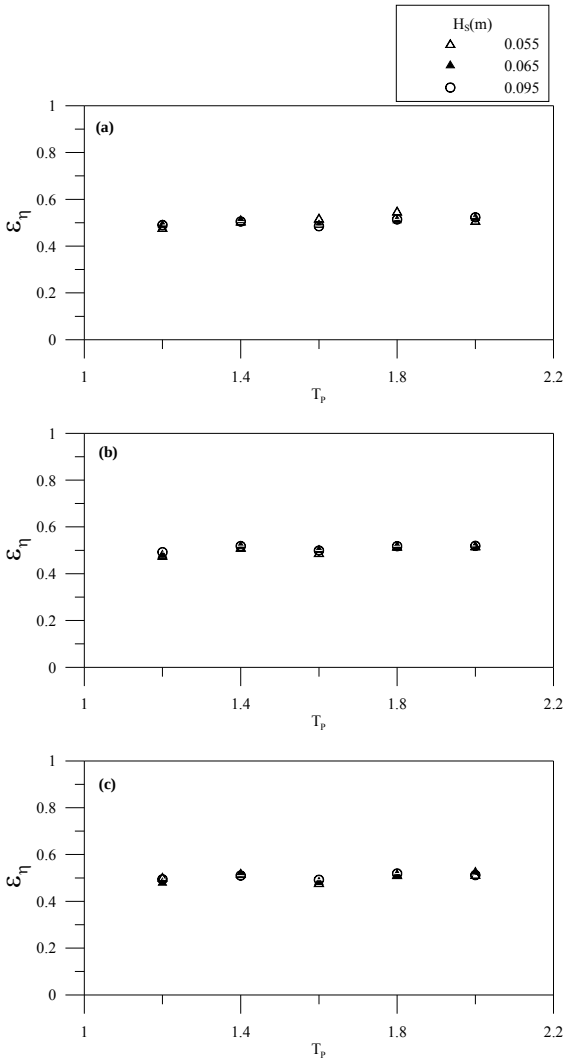

Figure 16: Spectral width of the incident wave at (a) b/B=0.25, (b) b/B=0.50 and (c) b/B=0.75.

The spectral energy ratio for rear wall pressure is plotted in Figs.21a-c brings out the effect of asymmetry and relative opening depth. Here the trend appears in inverse proportion to the one observed for front wall pressure. It is apparent that b/B=0.50 and O/d_i=0.45 produces favourable phase control effect in energy conversion. In the same manner, the energy ratios for air pressures are plotted in Figs.22a-c. This figure also supports the claims made over b/B and O/d_i in the foregoing sections.

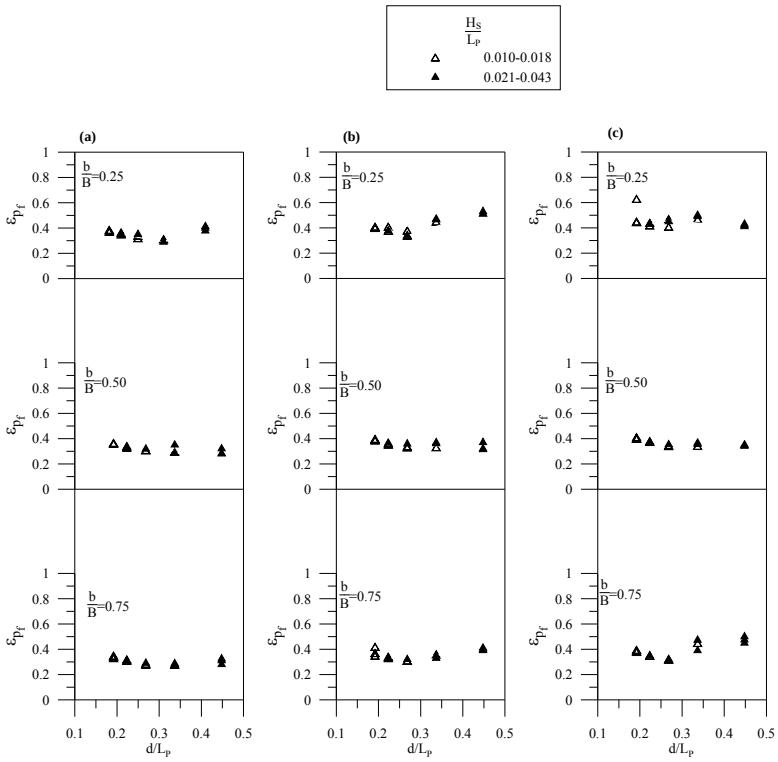

Figure 17: Effect of asymmetry on spectral width of the front wall pressure at (a) O/d_i=0.15, (b) O/d_i=0.30 and (c) O/d_i=0.45

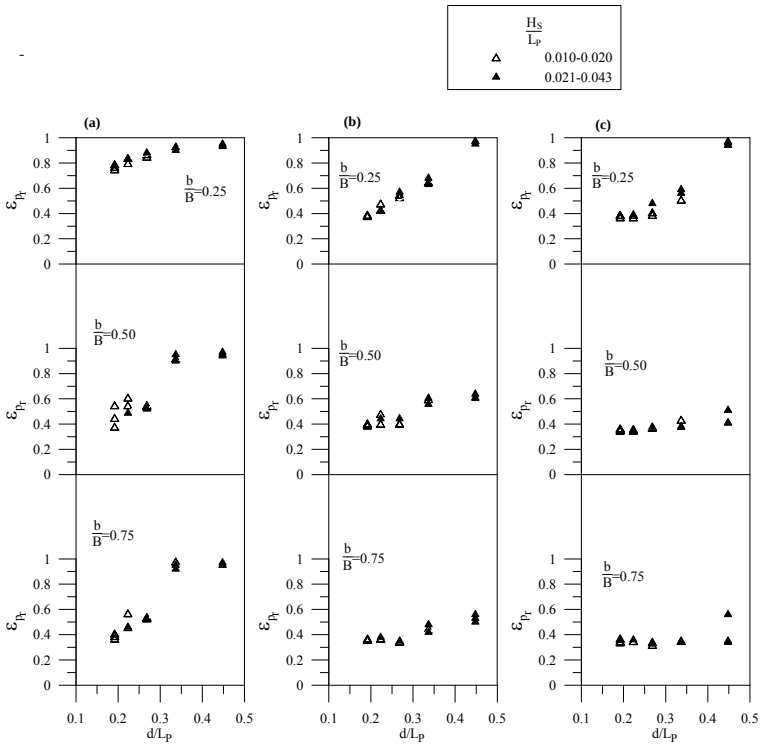

Figure 18: Effect of asymmetry on spectral width of the rear wall pressure at (a) O/d_i=0.15, (b) O/d_i=0.30 and (c) O/d_i=0.45

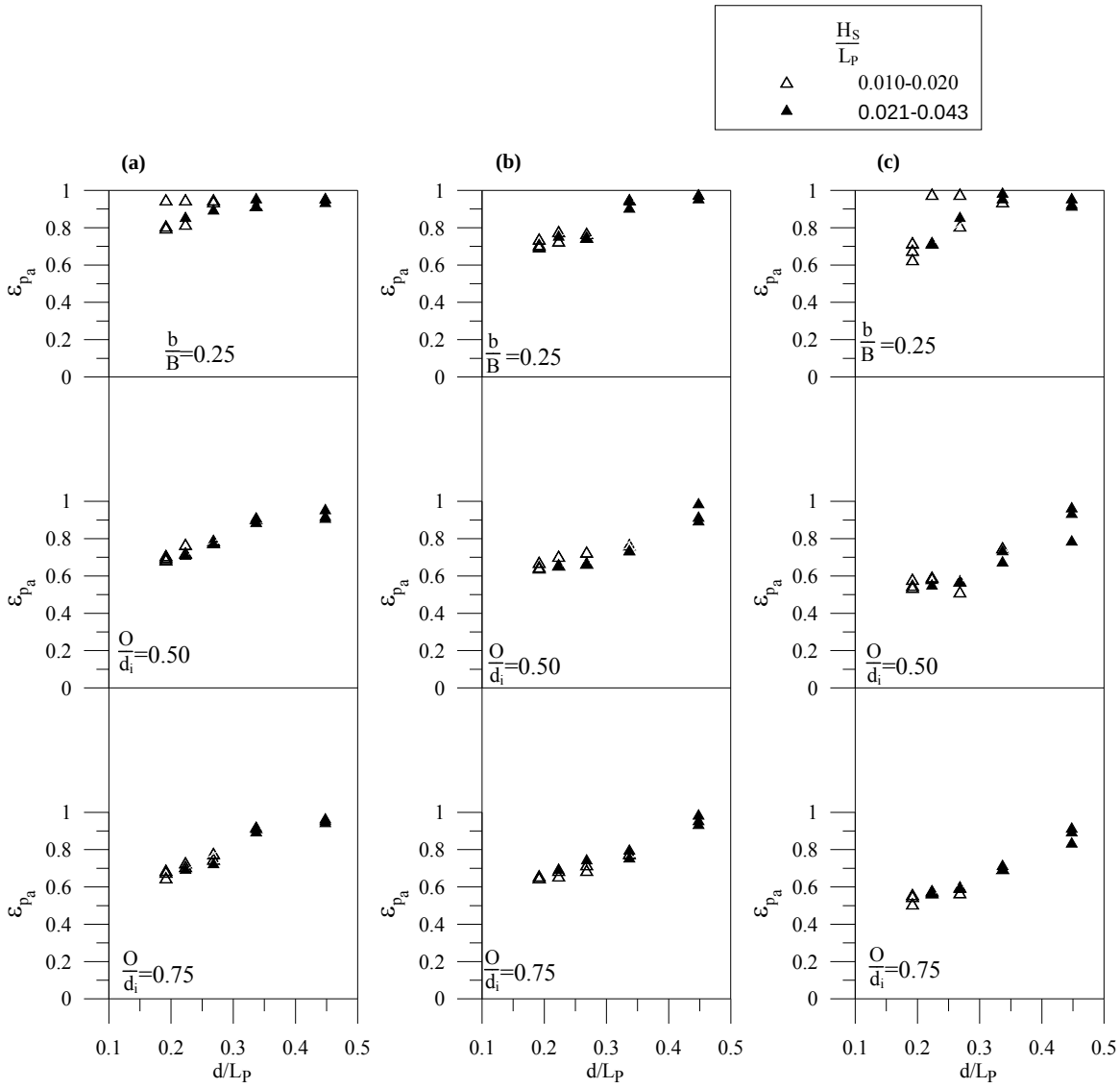

Figure 19 Effect of asymmetry on spectral width of the air pressure at (a) O/d_i=0.15, (b) O/d_i=0.30 and (c) O/d_i=0.45

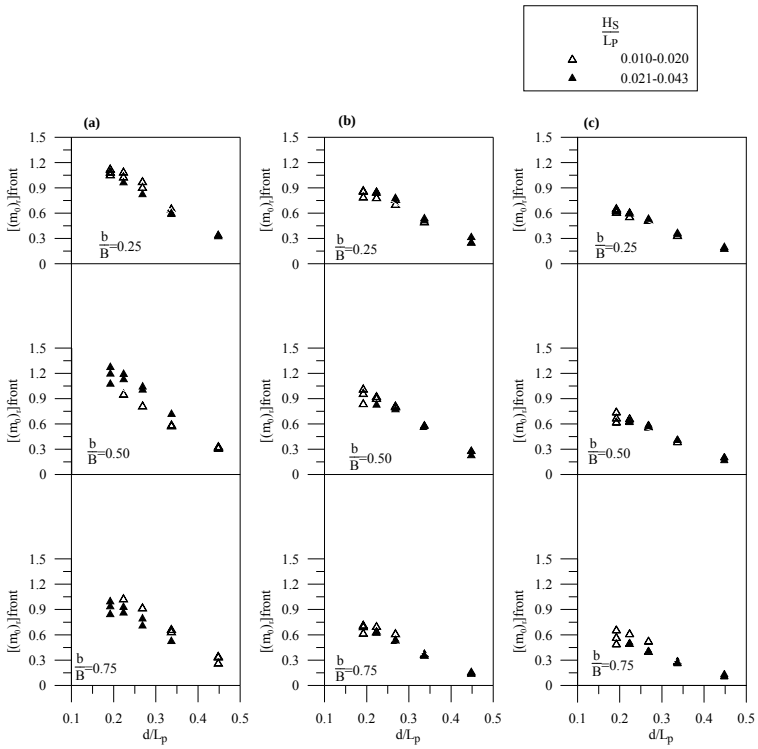

Figure 20: Effect of asymmetry on spectral energy of front wall pressure at (a) O/d_i=0.15, (b) O/d_i=0.30 and (c) O/d_i=0.45.

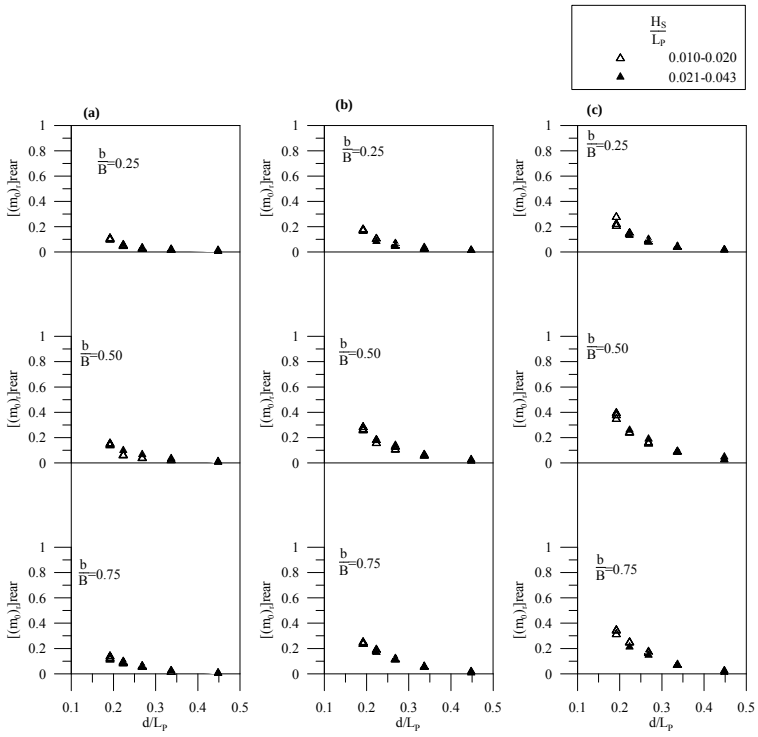

Figure 21: Effect of asymmetry on spectral energy of rear wall pressure at (a) O/d_i=0.15, (b) O/d_i=0.30 and (c) O/d_i=0.45.

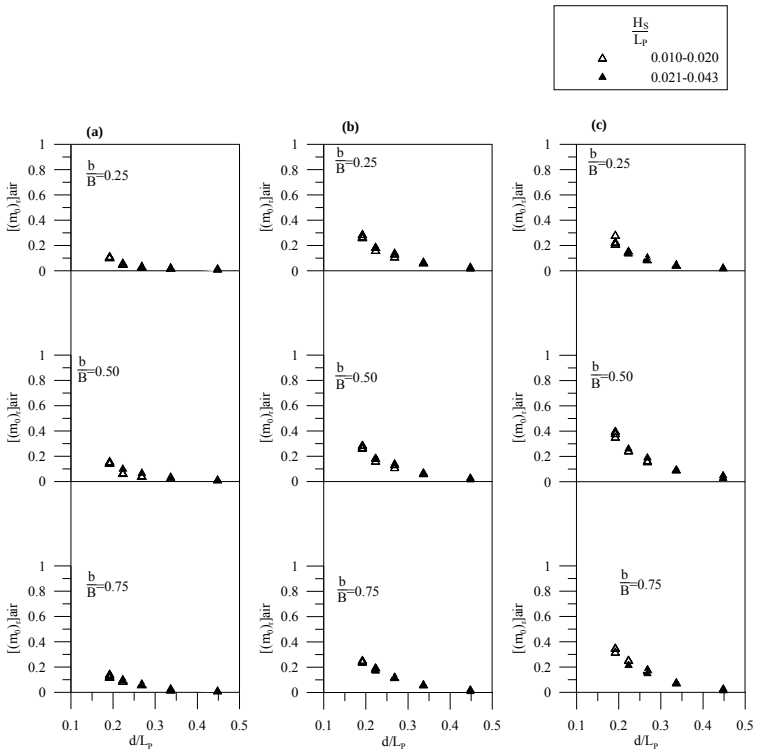

Figure 22: Effect of asymmetry on spectral energy of air pressure at (a) O/d_i=0.15, (b) O/d_i=0.30 and (c) O/d_i=0.45.

4. CONCLUSIONS

DCOWC is the new concept to achieve efficiency and effectiveness in energy conversion from waves. Though its principle of operation has been studied extensively by Boccotti [13,14], proportioning of geometric details remains unaddressed. The present study considers the influence two parameters namely; bottom opening depth and width of the front duct normal to the wave crest. Wave conditions of both regular and random were considered. It was observed that relative opening depth along with asymmetry value is having strong effect on hydrodynamic energy conversion capacity of the device. The important findings of the study are

- The piston movement of water surface inside the energy conversion chamber can be obtained by maintaining B/L=0.10, where B is the width normal to wave crest and L is the wave length.
- The energy conversion reaches optimum level for the asymmetry b/B=0.50, for lower values wave reflection predominates and for higher values attenuation over wave forcing is about to occur.
- The energy conversion reaches around 80% of the incident wave energy nearer the resonance condition.
- Resonance condition can be obtained by suitable combination of geometric parameters so that natural frequency of the device becomes equal to the wave frequency.

REFERENCE

1. Hagerman, G. (1995). A standard economic assessment methodology for renewable ocean energy projects, *Proceedings of the International Symposium on Coastal Ocean Space Utilization* (COSU'95), 129-138.
2. Sundar, V., Torgeir, M. and Jorgen, H. (2010). Conceptual Designs on Integration of Oscillating Water column Devices in Breakwaters, *Proc of the ASME 2010 29th Intl Conf on Ocean, Offshore and Arctic Eng OMAE2010*, pp 479-489
3. Falcao, A.F.D. (2010). *Wave energy utilization: A review of the technologies*. Renewable and Sustainable Energy Reviews, 14, 899–918.
4. Masuda, Y. (1979). Experimental Full Scale Result of Wave Power Machine Kaimei in 1978. *Symposium on Wave Energy Utilization Gothenburg*, October.
5. Ambli, N., Bonke, K., Malmo, O. and Reitan, H.(1982). The Kvaerner multiresonant OWC, *Proceedings of the 2nd International Symposium on wave Energy Utilisation*, Trondheim, Norway, Tapir, pp 275-295.
6. Count, B.M. and Evans, D.V.(1984).*The influence of projecting side walls on the hydrodynamic performance of wave energy devices*, Journal of Fluid Mechanics*:* 1984, 145, pp 361-376.
7. Malmo, O. and Reitan, A. (1986). *Wave power absorption by an oscillating water column in a reflecting wall*, Applied Ocean Research: 8(1), 42-48

8. McIver, P. and . D.V (1988). *An approximate theory for the performance of a number of wave energy devices set into a reflecting wall*. Applied Ocean Research,10(2), 58-65.
9. Zheng, W. (1989). Experimental Research and parameters optimization of a prototype OWC wave power device, *Proceedings of the International Conference on Ocean Energy Recovery '89*, pp 43-50.
10. Evans, D.V. and Porter, R. (1995). *Hydrodynamic characteristics of an oscillating water column device*, Applied Ocean Research, 18, pp155-164.
11. Ma. Q.W. (1995). Nonlinear analysis of hydrodynamic performance of oscillating water column wave energy device with a lateral opening, *Offshore Mechanics and Arctic Engineering Conference* Copenhagen, Denmark.
12. Korde, U.A. (1999). *Efficient primary energy conversion in irregular waves*. Ocean Engineering, 2, 625-651.
13. Boccotti, P. (2007). *Caisson breakwaters embodying an OWC with a small opening –Part I*: Theory, Ocean Engineering: 34, pp 806-819.
14. Boccotti, P., Filianoti, P., Fiamma, V. and Arena, F. (2007) *Caisson breakwaters embodying an OWC with a small opening-Part II: A small -scale field experiment*, Ocean Engineering*:* 34, pp 820-841.
15. Sarmento, A., and Thomas, G. (1993). Laboratory Testing of Wave Energy Devices, Wave Energy Converters Generic Technical Evaluation Study, *Annex Report B1, Device Fundamentals/Hydrodynamics*. C.E.C., Brussels.
16. Wang, D. J., Katory, M. and Li, Y.S. (2002). *Analytical and experimental investigation on the hydrodynamic performance of onshore wave-power devices*, Ocean Engineering 29, pp 871-885.
17. Thiruvenkatasamy, K. and Neelamani S. (1997). *On the efficiency of wave energy caisson in array*. Journal of Applied Ocean Research., Vol.19, pp 61-72.
18. Rapaka, E.V**.** (2007). Experimental investigation on a moored oscillating water column (MOWC) wave energy device, *Ph.D. thesis,* Ocean Engineering Department, Indian Institute of Technology Madras, Chennai.
19. Falnes, J. (2005). Ocean waves and oscillating systems. *Cambridge University Press*, ISBN 1139431935.
20. Koola P.M., Ravindran M. and Aswatha Narayan P.A. (1995). *Model studies of Oscillating Water Column Wave energy device.* Journal of Energy Engineering, 121, 14-27.
21. Zhang, Y., Zou, Q.P. and Greaves, D. (2012). *Air-water two phase flow modeling of hydrodynamic performance of an oscillating water column device,* Renewable Energy**.** 41**,** 159-170.

Journal of Ocean, Mechanical and Aerospace
-Science and Engineering-, Vol.5

March 20, 2014

Numerical Visualization of Rudder Inflow as Effect of Increasing Angle of Attack

Najmi. S.M.[a] , Priyanto. A.[a,*], Yasser. M.[a] and Maimun. A[a]

[1]*Marine Technology Centre, Universiti Teknologi Malaysia, 81310 UTM Skudai, Johor, Malaysia*

*Corresponding author: agoes@utm.my

Paper History

Received: 8-January-2014
Received in revised form: 1-March -2014
Accepted: 5-March-2014

ABSTRACT

Thispaper presents a study to examine the characteristics of the rudder inflow (propeller slipstream) using FLUENT v.6 visualization technique. The rotating propeller of 5 blades and semi-spade rudder were set in a uniform flow condition. The rudder distorts the angle-of-attack (AoA) or incident angle to the leading edge of the rudder blade. Time-averaged pressure and velocity field are proposed to analyze the AoA and show similar AoA values of 0°–7° at the region on rudder. However, it increases to 20° by those effects as the inflow comes to the rudder. From the AoA analysis the similar flow pattern is found to be about 7° in terms of the rudder angle. Cautious access is additionally necessary to introduce a reasonable safety against those inflow phenomena that would significantly influence the durability of the rudder.

KEY WORDS: *Rudder Inflow; Angle of Attack; Propeller Slipstream; FLUENT; Velocity Field.*

1.0 INTRODUCTION

Systematic prediction of propulsion system design is crucial towards efficient propulsion. Mainly contributed by the propeller, it is thrusting forward by screw movement and flow passing these twisted edges surrounding it. The hydrodynamic analysis of rotating propeller in vicinity of a rudder is somewhat a complex one. It has become one of the most challenging problems in computational fluid dynamics (CFD) validation [1], [2] and it has been investigated conventionally using potential theory for decades. As the year progressing, CFD has now become a practical tool in solving propeller flow problems via Reynolds Averaged Navier Stokes (RANS) solver. As ships are becoming larger and their power consumption is also increasing, high axial momentum behind a ship propeller may induce strong cavitation on the surface or discontinuities in the ship rudder. The propeller wake intrinsically has the contracted slipstream tube in the condition of uniform flow. However, it has specific angles of attack to the left (port) and right (starboard) sides of the rudder blade, which is located behind a propeller as validated by Kim, et.al [2] as shown in Fig.1.

Figure 1.a): Flow paint streaks on the port side of rudder [2]

Figure 1.b): Flow paint streaks on the starboard side of rudder [2]

The differences in incident flows toward the rudder have affected its lift forces and ships' manoeuvrability. To obtain sufficient lift forces in the rudder, an excessive rudder angle may be required in the actual operation of ship. On the other hand, an increased rudder angle induces a large amount of violent rudder cavitation, and may cause cavitation erosion of its surface. Securing sufficient lift has often conflicted with the trials of reducing rudder cavitation in both full-spade and semi-spade rudders. Rudder cavitation could have a negative effect on ships from hydrodynamic and structural viewpoints. If strong cavitation on the rudder results in serious damage, considerable time and cost would be necessary to maintain or repair a rudder eroded by cavitation. Therefore, it is very important to inspect flow behaviour around the rudder when the propeller is ahead of the

rudder.

2.0 PROPELLER AND RUDDER

A five bladed B-series typed B 5-88 propeller is considered. The propeller is intended to propel the LNG carrier. It is a fixed pitch and the axis of the propeller is parallel with the free stream direction. The extistance of hull as shown in Fig.2 was used to simulate the non-uniform incoming wake pattern. In the simulation, the non-uniform wake pattern was defined to replace the available default function in the Ansys FLUENT. The placement of hull before propeller and rudder hence should make an adequate simulation results due to the defined non-uniform wake source.

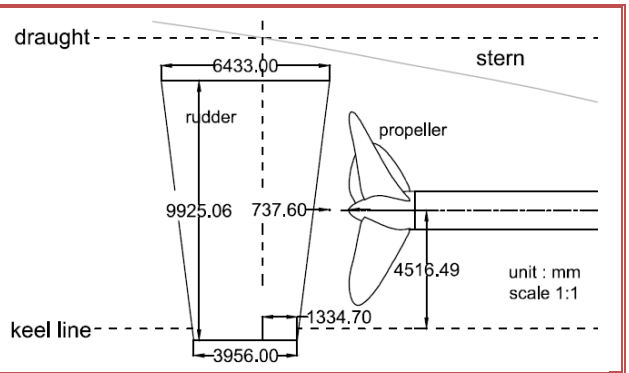

Figure 2: Sketch of semi-spade rudder incident flow caused by propeller wake

3.0 MODELING SET UP

As dealing with complex geometry like propeller and rudder, it is quite difficult for direct simulation of turbulence. Using time averaged technique such as Reynolds Averaged Navier Stokes (RANS), it is used to simplify the instantaneous RANS [3]. The equations are as following:

$$\rho \frac{\partial u_i}{\partial x_i} = 0 \tag{1}$$

$$\rho \frac{\partial}{\partial x_j}(u_i u_j) = -\frac{\partial p}{\partial x_i} + \rho \frac{\partial}{\partial x_j}\left[v\left(\frac{\partial u_i}{\partial x_j} + \frac{\partial u_j}{\partial x_i}\right)\right] - \frac{\partial}{\partial x_j}\left(-\rho \overline{u_i' u_j'}\right) \tag{2}$$

In which u_i and $u_j(i, j=1, 2, 3)$ are time averaged velocity components; x_i and $x_j(i,j= 1, 2, 3)$ are coordinates in surge, heave, and sway directions respectively; density of fluid (ρ), time averaged pressure (p), kinetic viscosity of water (υ), and Reynolds stress term $\left(-\rho \overline{u_i' u_j'}\right)$. For proceeding calculations, standard k epsilon turbulence model is used. The transport equations of standard k epsilon turbulence model are as follows:

$$\rho \frac{Dk}{Dt} = \frac{\partial}{\partial x_j}\left(\alpha_{k\mu_{eff}} \frac{\partial k}{\partial x_j}\right) + P - \rho\varepsilon \tag{3}$$

$$\rho \frac{D\varepsilon}{Dt} = \frac{\partial}{\partial x_j}\left(\alpha_{k\mu_{eff}} \frac{\partial k}{\partial x_j}\right) + C_{1\varepsilon}\frac{\varepsilon}{k}P - C_{2\varepsilon}\rho\frac{\varepsilon^2}{k} \tag{4}$$

In which k represents the turbulent kinetic energy, ε is dissipation ratio of k, t being time, while ρ and x_j are already defined in equation (1) and (2). μ_{eff} is the turbulent kinetic energy, P represents the production of turbulence kinetic energy. α_k= 1.0 and α_ε = 1.3 are the inverse effective Prandtl number of k and ε respectively, while $C_{1\varepsilon}$ = 1.44 and $C_{2\varepsilon}$= 1.92 act as constants of the model.

Table 1: Geometrical parameters of propeller and rudder

Items	symbol	value
diameter	*D*	7700mm
pitch-diameter ratio	*P/D*	0.94
expanded area ratio	A_E/A_O	0.88
number of blade	*z*	5
rudder height/*D*	*L/D*	1.289
rudder height/chord	482	565

Steady analysis of propeller-rudder interaction was analyzed using multiple reference frame method to simulate the interaction between the rotor and stator domains. The mesh elements consist of two parts; moving mesh and stationary mesh. Unstructured grids are used in both domains. The size of computational domain was referred to [4] for the open water test (OWT 1). A description to Fig. 3 is available in Table.2, where *Lmr* is measured from middle hub, *D* and *L* are referring to propeller diameter and domain length.

Table 2: Open Water Tests (OWT) computational domain

Items	OWT1 w/o rudder	OWT2 with rudder
Ds	3.6D	3.6D
Dr	1.4D	1.4D
Lsi	2D	2D
Lso	6D	6D
Lr	1.4D	0.75D
Lmr	0.7D	0.214D

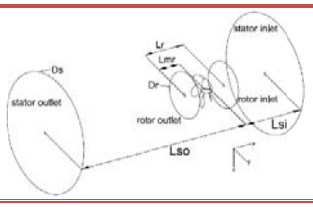

Figure 3.a): Computational configuration domain

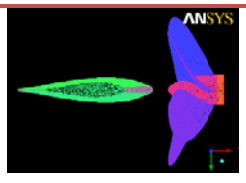

Figure 3.b): Definition of Angle of Attack AoA (α) ahead of rudder leading edge

The flow regions are assigned into several categories:

- The inlet – velocity inlet assumed, assigned value, the characteristic dimension and turbulence model values
- The outlet – pressure outlet is assumed
- Propeller blades and shaft – non viscous wall

- Outer boundary – non viscous wall.

Tests were performed at full scale. The rudder rests at three designated positions; AoA= 0^0,-7^0 and -20^0 positioned 0.0958D from top of hub as per classification requirement. Information regarding angle of attack is available in Fig. 3b). The solver setting was based on [1]. The advance speed, V_A was fixed at 6.687 m/s. The stator inlet was designated as velocity inlet, while the stator outlet was designated as pressure outlet with normal atmospheric pressure.

Regarding the solver setting, pressure based calculation with absolute velocity formulation and steady flow were selected. Total number of mesh elements for rudder AoA = 0^0,-7^0 and -20^0 are averaged at 1.8millions while OWT 1 and OWT 2 counts for 1.485 millions in average. Fluid domain was specified as fresh water and aluminium for solid domain.

Proceeding to solution methods, simple pressure-velocity coupling was selected with second order upwind for momentum turbulent kinetic energy and turbulent dissipation rate. Detailing the boundary conditions, velocity inlet was selected for stator inlet with intensity and viscosity ratio of 10 for the turbulent specification method. Pressure outlet is defined for the stator outlet with zero gauge pressure and similar turbulent specification as stator inlet. All convergence rests at 0.001.

4.0 RESULTS AND DISCUSSION

Figures 4 – 9 show that the pressure distribution at starboard side was higher than the one at port side, it means that the flow goes on the negative AoA. Time-averaged pressure field are proposed to analyze the AoA and show similar AoA values of 0°,–7° at the region on rudder. However, it increases to -20° by those effects as the inflow comes to the rudder. The maximum pressures are located at absolute Z = 0.7R near the upper rudder face view from port side and lower rudder face of starboard side. These may happen due to clockwise movement of the propeller slipstream. This is the phenomenon where tip vortices sourcing from propeller attacks rudder surface.

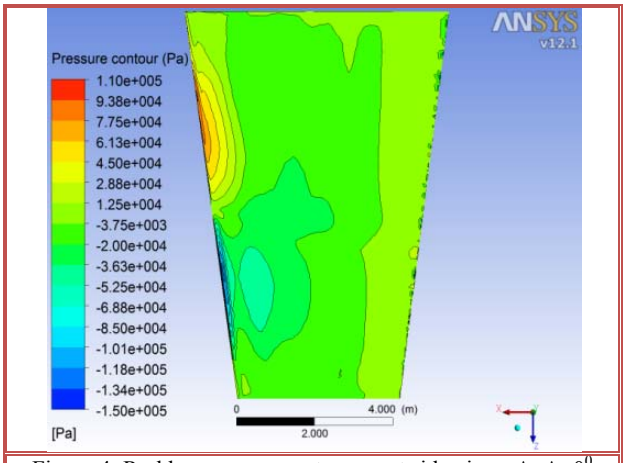

Figure 4: Rudder pressure contours port side views AoA=0^0

As the rudder deflects more, significant pressure drop can be noticed at absolute Z = 0.7R port side of rudder leading edge. This is likely the occurrence of cavitation inception, in which the lower pressure values as indicated in the Figures 5 and 6 have crucial effects on the cavitation and flow separation, as claimed by [4,5].

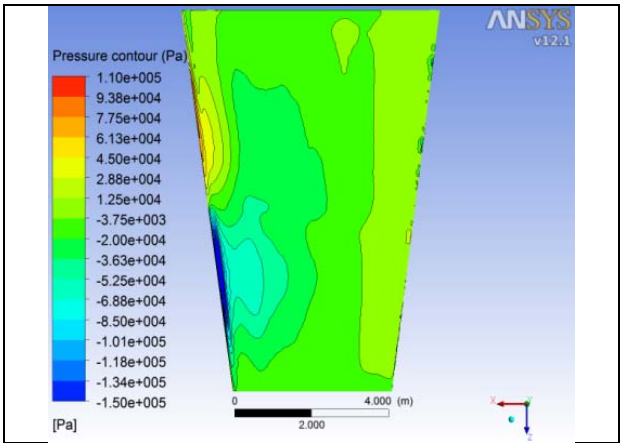

Figure 5: Rudder pressure contours port side views AoA=-7^0

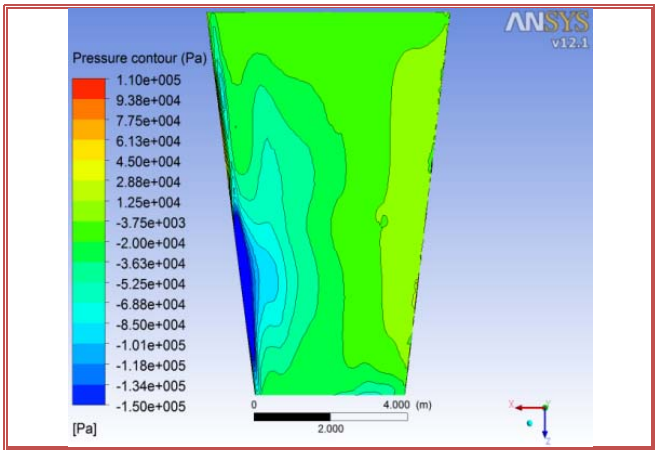

Figure 6: Rudder pressure contours port side views AoA=-20^0

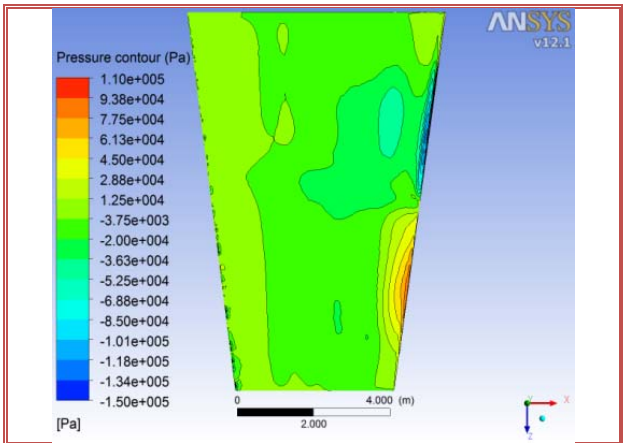

Figure 7: Rudder pressure contours starboard side views AoA=0^0

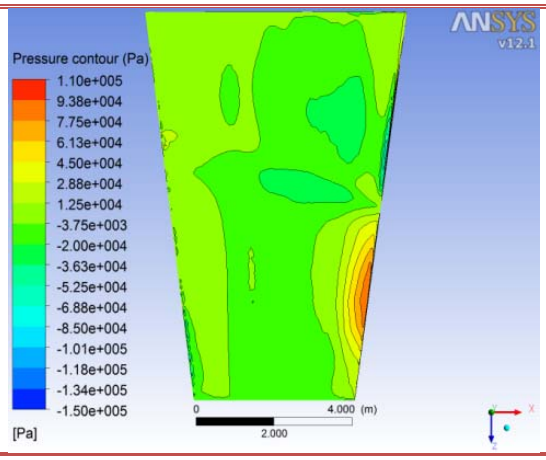

Figure 8: Rudder pressure contours port side views AoA=-7^0

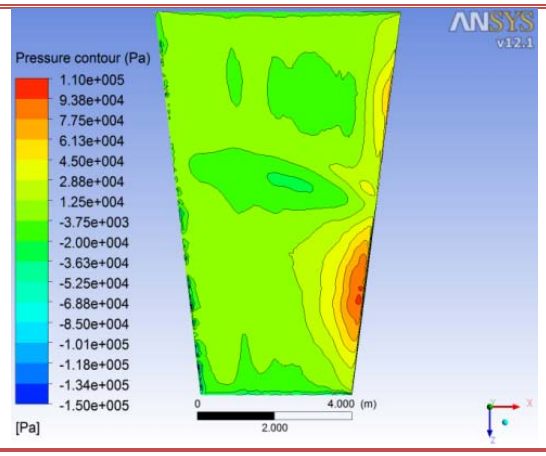

Figure 9: Rudder pressure contours port side views AoA=-20^0

Next Figs 10 – 12 represent rudder ambient velocity contours in XZ cross sectional plane positioned right after the rotational domain (X= -0.291m).

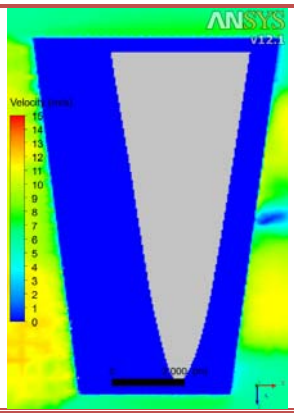

Figure 10: Velocity contours of surrounding fluids starboard side views at rudder angle AoA=0^0

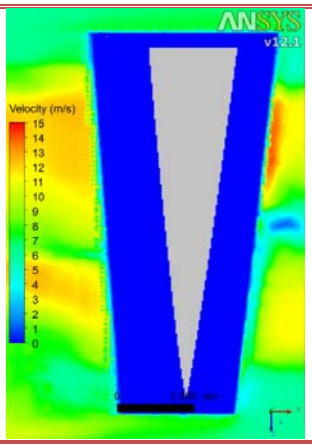

Figure 11: Velocity contours of surrounding fluids starboard side views at rudder angle AoA=-70^0

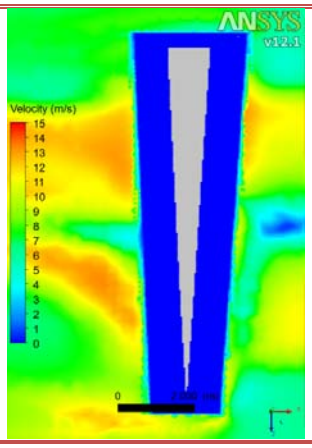

Figure 12: Velocity contours of surrounding fluids starboard side views at rudder angle AoA=-20^0

As we can see, significant amount of velocity difference are noticed at the region of Z = 0.7R, near top side of rotating propeller. The amount of velocity becomes larger as the rudder started to deflect and slightly lower as the rudder deflects to -20^0. An indicator of tip vortex cavitation may prevail here, in which regions of high velocity tailing from propeller tip is a sign of lower pressure compared to fluid at rest (Bernoulli's law).This may happen due to typically low advance velocity on the upper side of a rotating propeller, viewed from propeller back. High propeller blades angle of attack is the cause to the lower pressure and therefore experiences higher velocity.

5.0 CONCLUSION

The flow of propeller-rudder interaction has been investigated using RANS modelling. Significant differences in terms of induced velocity field and pressure distribution could be noticed. Prediction and inspection of flow behaviour could be made possible in order to locate the cavitation susceptibility as early

precaution to structural assessment of rudder. These characteristics are important for further assessment especially durability of propeller and strength assessment for safety manoeuvring. This moving reference frame method provides an adequate solution for the determination of time accurate solution to predict the propeller and rudder interaction.

ACKNOWLEDGEMENTS

All results were obtained from the research project "Modelling propeller and rudder induced forces for deep drafted vessels in Restricted Water". Thanks to Universiti Teknologi Malaysia (UTM) and Ministry of Higher Education (MOHE), Malaysia for the financial support to this project denoted by R.J130000.7824.4F049.

REFERENCE

[1] Mitja Morgut, E. N. (2009), Comparison of Hexa-Structured and Hybrid-Unstructured Meshing Approaches for Numerical Prediction of the Flow Around Marine Propellers, *First International Symposium on Marine Propulsors smp'09, Trondheim, Norway: 7*.

[2] Van, S.H., Kim, W.J., Yoon, H.S., Lee, Y.Y. (2006), *Flow measurement around a model ship with propeller and rudder*, Experiments in Fluids 40, Springer – Verlag: 533-545.

[3] Chun-yu Guo , W.-t. H. a. S. H. (2010), *Using RANS to Simulate the Interaction and overall Performance of Propellers and Rudders with Thrust Fins*, Journal of Marine Science and Application 9: 323-327.

[4] Jan Kulczyk, L. S., Maciej Zawiślak (2007), Analysis Of Screw Propeller 4119 Using The Fluent System, *Archives of Civil And Mechanical Engineering 7(4): 9*.

[5] Yavuz Hakan Ozdemira, S. B., Tamer Yılmaza (2009), Flowfield Analysis Of A Rudder By Using Computational Fluid Dynamics, *International Advanced Technologies Symposium (IATS'09), Karabuk, Turkey 5*.

Journal of Ocean, Mechanical and Aerospace
-Science and Engineering-, Vol.5

March 20, 2014

Semi-Submersible Heave Response Study Using Diffraction Potential Theory with Viscous Damping Correction

C.L Sow [a], Jaswar Koto,[a,b,*] and Hassan Abyn,[a]

[a)] *Mechanical Engineering, Universiti Teknologi Malaysia*
[b)] *Ocean and Aerospace Research Institute, Indonesia*

*Corresponding author: jaswar.koto@gmail.com

Paper History

Received: 5-February-2014
Received in revised form: 10-March-2014
Accepted: 19-March-2014

ABSTRACT

This paper discussesthe numerical prediction of the semi-submersible's heave motion. In the previous study, it is observed that the heave motion response predicted by diffraction potential theory is over-estimated in the region where the heave motion is dominated by damping. In this research, viscous damping is included in the calculation to increase the heave damping magnitude in motion equation. The wave force and added massof semi-submersible is predicted by diffraction potential theory, only the total damping is corrected by sum-up the linear damping from diffraction potential theory with the proposed viscous damping. The heave motion response obtained from the proposed numerical method also compared to the data from the experiment. From the comparison, it can conclude that involved of viscous damping in the calculation will corrected a part of heave motion response tendency and reduce the large over-predicted error of heave motion response at the damping dominate.

KEY WORDS:*Diffraction Potential, Viscous Damping, Heave Motion, Semi-Submersible.*

NOMENCLATURE

$\Phi(x,y,z)$	Wave Potential
A_{ij}	Added Mass
B_{ij}	Linear Damping
$G(P;Q)$	Green Function
ν	Damping Ratio
w_n	Natural Frequency
E_i	Wave Force
δ	Logarithm Decrement
w_d	Damped Natural Frequency
n_i	Normal Vector

1.0 INTRODUCTION

This work proposes a damping correction method for linear diffraction theory in order to evaluate the heave motion response of selected offshore floating structure correctly. The linear diffraction theory estimate the wave force on the floating body based on frequency domain and this method can be considered as an efficient method to study the motion of the large size floating structure with acceptable accuracy. This is because previous study also observed that the diffraction effect is significant for the large structure [16]. However, the offshore structure such as semi-submersible, TLP and spar are looked like a combination of several slender bodies as an example, branching for semi-submersible.

In this study, semi-submersible structure is selected as an offshore structure model because this structure is one of the flavoursstructures used in deep water oil and gas exploration area. To achieve this objective, a programming code was developed based on diffraction potential theory and it is written in visual basic programming language. By comparing the numerical result executed by using diffraction potential theory to experiment result, it is obtained that this theory able to predict the motion response for semi-submersible with acceptable accuracy most of the time, except for heave motion when the wave frequency near to the structure natural frequency [17].

As presented in previous paper, diffraction potential theory is less accurate to predict the structure heave motion response when the wave frequency closer to structure natural frequency. At this situation, the heave response calculated by the diffraction

potential theory will be overshooting to infinity compare to experiment result due to low damping executed by the theory. However, the diffraction potential theory still able to catch the heave response accurately other than damping dominate region [17].

In order to correct the over-predicting phenomenon made by the diffraction potential theory, this research wastrying to increase the damping coefficient by adding viscous damping into the motion equation. From that study, the viscous damping is treated as extra matrix and can be added into the motion equation separately. This addition viscous damping was estimated based on the equation proposed by S. Nallayarasu and P. Siva Prasad in their published paper [19].

Accuracy of this modification solution was also checked with the previous semi-submersible experiment result which carried out at towing tank belongs to University Teknologi Malaysia [12, 18]. The experiment is conducted in head sea condition and slack mooring condition for wavelengthfrom 1 meter to 9 meters. The comparison obtained that by adding the extra viscous damping into the motion equation, it can reduce error on the significant over-predicting of heave motion at the situation when wave frequency near to the semi-submersible natural frequency.This alsocaused the predicted motion response tendency is closed to the experimental result compared to executed result by diffraction potential theory alone.Besides, this paper will discuss the proposed viscous damping equation in the beginning and then the effect addition viscous damping change the motion equation.The difference of heave response results obtained from diffraction potential theory with the existing of viscous damping and without viscous damping is also discussed here.

2.0 LITERATURE REVIEW

Hess and Smith, Van Oortmerssen and Loken studied on non-lifting potential flow calculation about arbitrary 3D objects [1, 2, 3]. They utilized a source density distribution on the surface of the structure and solved for distribution necessary to lake the normal component of fluid velocity zero on the boundary. Plane quadrilateral source elements were used to approximate the structure surface, and the integral equation for the source density is replaced by a set of linear algebraic equations for the values of the source density on the quadrilateral elements. By solving this set of equations, the flow velocity both on and off the surface was calculated. Besides, Wu et al. also studied on the motion of a moored semi-submersible in regular waves and wave induced internal forces numerically and experimentally [4]. In their mathematical formulation, the moored semi-submersible was modelled as an externally constrained floating body in waves, and derived the linearized equation of motion.

Comparison between the capability of potential theory and viscous fluid theory to predict the fluid characteristic in the narrow gaps between the floating bodies was studied by Lin Lu et.al. Their simulation result showed that the potential theory over predicted the fluid resonance amplitude but it can correct by modifying the theory with included artificial damping term, μ=0. 4~0.5 [18].

Yilmaz and Incecik analyzed the excessive motion of moored semi-submersible [5]. They developed and employed two different time domain techniques due to mooring stiffness, viscous drag forces and damping. In the first technique, first-order wave forces acting on structure which considered as a solitary excitation forces and evaluated according Morison equation. In second technique, they used mean drift forces to calculate slowly varying wave forces and simulate for slow varying and steady motions. Söylemez developed a technique to predict damaged semi-submersible motion under wind, current and wave [6]. He used Newton's second law for approaching equation of motion and developed numerical technique of nonlinear equations for intact and damaged condition in time domain.

Clauss et al. analyzed the sea-keeping behavior of a semi-submersible in rough waves in the North Sea numerically and experimentally [7]. They used panel method TiMIT (Time-domain investigations, developed at the Massachusetts Institute of Technology) for wave/structure interactions in time domain. The theory behind TiMIT is strictly linear and thus applicable for moderate sea condition only.

An important requirement for a unit with drilling capabilities is the low level of motions in the vertical plane motions induced by heave, roll and pitch. Matos et al. were investigated second-order resonant of a deep-draft semi-submersible heave, roll and pitch motions numerically and experimentally [8]. One of the manners to improve the hydrodynamic behavior of a semi-submersible is to increase the draft. The low frequency forces computation has been performed in the frequency domain by WAMIT a commercial Boundary Element Method (BEM) code. They generated different number of mesh on the structure and calculated pitch forces.

Due to the complexity of actual structures' hull form, S. Nallayarasu and P. Siva Prasad were used experimental and numerical software (ANSYS AQWA) to study the hydrodynamic response of an offshore spar structure which linked to semi-submersible under regular waves. From both the experimental and numerical result, it is obtained that the response of the spar is reduced after linked to semi-submersible due to the interaction of radiation wave generated by both the structures and the motion of spar may be reduced by semi-submersible. However, the research also obtained that the motion response for unmoored semi-submersible is increased when linked to spar [19].

Wackers et al. was reviewed the surface descretisation methods for CFD application with different code [9]. Besides, simulation of fluid flow Characteristic around Rounded-Shape FPSO was also conducted by A. Efi et al. using RANs Method [10]. Jaswar et al. were also developed integrated CFD simulation software to analyze hull performance of VLCC tanker. The integrated CFD simulation tool was developed based on potential theory and able to simulate wave profile, wave resistance and pressure distribution around ship hull [11].

In addition, few experiment tests were carried out to obtain the motion response of semi-submersible. A model test related to interaction between semi-submersible and TLP was carried out by Hassan Abyn et al. [12]. In continue Hassan Abyn et al. also tried to simulate the motion of semi-submersible by using HydroSTAR and then analyse the effect of meshing number to the accuracy of execution result and execution time [13]. Besides, C. L. Siow et al. also make a comparison on the motion of semi-submersible when it alone to interaction condition by experimental approach [14]. Besides that, K.U. Tiau (2012) was simulating the motion of mobile floating harbour which has similar hull form as semi-

submersible by using Morison Equation [15].

3.0 MATHEMATICAL MODEL

3.1 Diffraction Potential

In this study, diffraction potential theory was used to obtain the wave force act on the semi-submersible structure, added mass and damping for all six directions of motions. The regular wave acting on floating bodies can be described by velocity potential. The velocity potential normally written in respective to the flow direction and time as below:

$$\Phi(x,y,z) = Re[\phi(x,y,z)e^{iwt}] \quad (1)$$

$$\phi(x,y,z) = \frac{g\varsigma_a}{iw}\{\phi_0(x,y,z) + \phi_7(x,y,z)\} + \sum_{j=1}^{6} iwX_j\phi_j(x,y,z) \quad (2)$$

where; g is gravity acceleration, ς_a is incident wave amplitude, X_j is motions amplitude, ϕ_0 is incident wave potential, ϕ_7 is scattering wave potential, ϕ_j is radiation wave potential due to motions and j is direction of motion.

From the above equation, it is shown that total wave potential in the system is contributed by the potential of the incident wave, scattering wave and radiation wave. In addition, the phase and amplitude for both the incident wave and scattering wave is assumed to be the same. However, radiation wave potentials are affected by each type of motion of floating body inside system, where the total potential for radiation wave for the body is the summation of the radiation wave generates by each type of body motion such as roll, pitch, yaw, surge, sway and heave.

The diffraction wave potential $\emptyset^{(d)}$ must be satisfied with boundary conditions as below:

$$\nabla^2\emptyset^{(d)} = 0 \quad for\ 0 \le z \le h \quad (3)$$

$$\frac{\partial\emptyset^{(d)}}{\partial z} + k\emptyset^{(d)} atz = 0 \quad (k = \frac{w^2}{g}) \quad (4)$$

$$\frac{\partial\emptyset^{(d)}}{\partial z} = 0 \qquad atz = h \quad (5)$$

$$\emptyset^{(d)} \sim \frac{1}{\sqrt{r}} e^{-ik_0 r} shouldbe\ 0\ if r\infty \quad (6)$$

$$\frac{\partial\emptyset^{(d)}}{\partial n} = -\frac{\partial\emptyset_0}{\partial n} onthebodyboundary \quad (7)$$

3.2 Wave Potential

By considering the wave potential only affected by structure's surface, S_H, the wave potential at any point can be presented by following equation:

$$\emptyset(P) = \iint_{S_H}\left\{\frac{\partial\emptyset(Q)}{\partial n_Q}G(P;Q) - \emptyset(Q)\frac{\partial G(P;Q)}{\partial n_Q}\right\}dS(Q) \quad (8)$$

where $P = (x, y, z)$ represents fluid flow pointed at any coordinate and $Q = (\xi, \eta, \varsigma)$ represent any coordinate, (x, y, z) on structure surface, S_H. The green function can be applied here to estimate the strength of the wave flow potential. The green function in eq. (8) can be summarized as follow:

$$G(P;Q) = -\frac{1}{4\pi\sqrt{(x-\xi)^2 + (y-\eta)^2 + (z-\zeta)^2}} + H(x-\xi, y-\eta, z+\zeta) \quad (9)$$

where; $H(x-\xi, y-\eta, z+\zeta)$ in eq. (9) represent the effect of free surface and can be solved by second kind of Bessel function.

3.3 Wave Force, Added Mass and Damping

The wave force or moment acts on the structure to cause the motions of structure can be obtained by integral the diffraction wave potential along the structure surface.

$$E_i = -\iint_{S_H}\phi_D(x,y,z)n_i dS \quad (10)$$

where; ϕ_D is diffraction potential, $\phi_D = \phi_o + \phi_7$

Also, the added mass, A_{ij} and damping, B_{ij} for each motion can be obtained by integral the radiation wave due to each motion along the structure surface.

$$A_{ij} = -\rho\iint_{S_H} Re[\phi_j(x,y,z)]n_i dS \quad (11)$$

$$B_{ij} = -\rho w\iint_{S_H} Im[\phi_j(x,y,z)]n_i dS \quad (12)$$

n_i in eq. (10) to eq. (12) is the normal vector for each direction of motion, i = 1~ 6 represent the direction of motion and j = 1~6 represent the six type of motions

3.4 Viscous Damping

The modified viscous damping from the equation provided by S. Nallayarasu and P. Siva Prasad [19] is shown asfollows expression:

$$b_v = \nu\,[(M + A_{33})w_n]\,C \quad (13)$$

Where b is heave viscous damping of the floating structure, ν is damping ratio for heave, M is the mass of the floating structure, A_{33} is heave added mass of floating structure and it is calculated from diffraction potential theory and w_n is heave natural frequency and C is the constant for the viscous damping.

The damping ratio, ν and heave natural frequency, ω at the equation (13) can be found from heave decay experiment. Based on the result obtained from heave decay experiment, the logarithmic decrement method which defines the natural log of the amplitude of any two peaks can be used to find the damping ratio of an under-damped system. The equation for the logarithmic decrement, δ as follows

$$\delta = \frac{1}{n}\ln\left(\frac{x_0}{x_n}\right) \quad (14)$$

where x_0 is the first peak amplitude and x_n is the n-th peak amplitude. After the logarithmic decrement, δ found, the damping ratioν can be found from the following equation:

$$\nu = \frac{\delta}{\sqrt{\delta^2 - 4\pi^2}} \quad (15)$$

Besides, the heave decay experiment also can be used to obtain the damped natural frequency, w_d and heave natural frequency, w_n by following equation:

$$w_d = \frac{2\pi}{T} \quad (16)$$

$$w_n = \frac{w_d}{\sqrt{1-\varsigma^w}} \quad (17)$$

where the variable T is period of heave oscillation motion or time required for two continue successive amplitude peaks.

By insert the data obtained from heave decay experiment into equation (13) the heave viscous damping will able to calculate and insert into the motion equation follow:

$$(M + A_{33})\ddot{X}_z + (B_{33} + b_v)\dot{X}_z + cX = F \quad (18)$$

where the M is structure mass, A_{33} is heave added mass, $B_{33}$is linear damping from diffraction potential theory, $b_v$is the viscous damping defined at equation (13), c is the heave restoring force, and F is the wave force contributed to heave motion.

3.0 MODEL PARTICULAR

As mentioned, the semi-submersible model was selected as the test model in this study. This Semi-submersible model was constructed based on GVA 4000. The model is constructed from four circular columns connected to two pontoons and two braces. Two pieces of plywood are fastened to the top of the Semi-submersible to act as two decks to mount the test instruments. The model was constructed from wood following the scale of 1:70 (Table 1).

Upon the model complete constructed, few tests were carried out to obtain the model particulars. Inclining test, swing frame test, oscillating test, decay test and bifilar test were carried out to identify the hydrostatic particular for the semi-submersible. The dimension and measured data for the model was summarized as in table 1.

Table 1 Principal particular of the Structures.

Length	0.954 m
Width	0.835 m
Draft	0.239 m
Displacement	0.043501 m^3
Water Plan Area	0.108082 m^2
Number of Columns	4
Pontoon length	0.954 m
Pontoon depth	0.09 m
Pontoon width	0.19 m
Pontoons centerline separation	0.645 m
Columns longitudinal spacing (centre)	0.651143 m
Column diameter	0.151286 m
GM_T	0.041 m
GM_L	0.058 m
K_{XX}	0.452 m
K_{YY}	0.385 m
K_{ZZ}	0.5 m

4.0MESHING FOR SEMI-SUBMERSIBLE

In this study, the numerical method applies to executing the motion response of semi-submersible will only estimate the wave force acting on the surface of the port side structure of semi-submersible. After that, the total wave force for the semi-submersible is double before it fixed into the motion equation.

The selected semi-submersible model in this study is constructed based on GVA 4000 type. Total panels used in the execution are 272 where 25 panels on each column and 222 panels on pontoon surface. The example meshing constructed by this numerical method for the semi-submersible model is shown in figure 1.

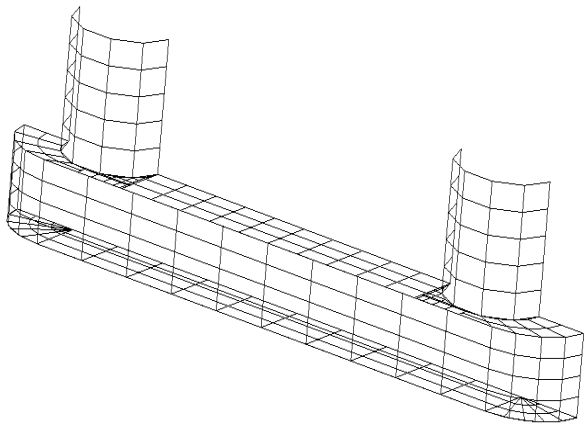

Figure 1: Meshing for semi-submersible model

5.0 RESULT

5.1 Heave Decay Experiment

The heave decay experiment was carried out to collect the required data, such as damping ratio and natural heave frequency to able the programming to execute the heave viscous damping. This decay experiment was carried out by displacing the model in the heave directions or along the heave axes, releasing and recording the displacement time histories. The tests are repeated when necessary to obtain reliable results. The data collected from decay experiment after that was processed to obtain the required information for the execution of heave viscous damping follow the discussion in part 3.4. From the calculation, it is obtained that the heave damping ratio, ν is 1.628 %, while the heave natural frequency is 3.23 rad/Secin model scale. The time domain heave decay data collected from the experiment is shown in figure 2.

5.1 Heave Motion Response

In this part, the heave response amplitude for GVA 4000 semi-submersible structure in head sea condition was discussed. The result from the proposed numerical result was also compared to the motion experiment result. Input for the numerical program was also adjusted to make the condition as close as the experimental condition. Since this paper is targeted to discuss the involving of viscous damping in calculation to correct the heave

motion predicted by the diffraction potential theory, thus the discussion will only made on the heave motion.

.

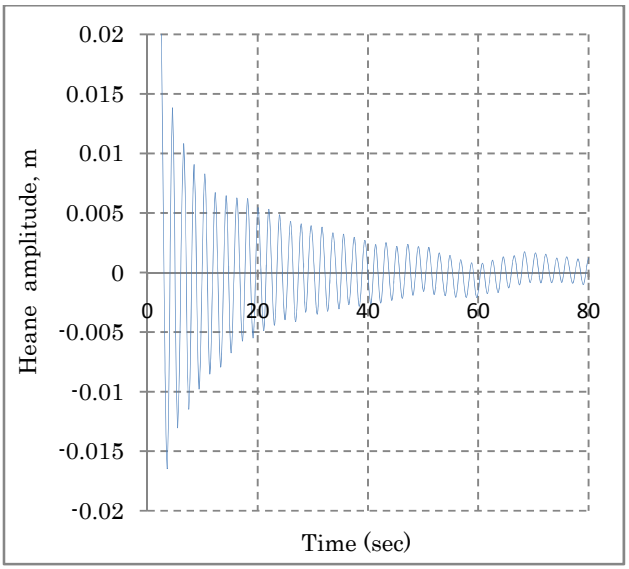

Figure 2: Heave amplitude for semi-submersible in the time domain for the heave decay experiment.

From the previous study, it can be obtained that the diffraction potential theory is weak in predicting the heave motion response when the wave frequency closes to the structure natural frequency. By detail study of the problem, it is obtained that the linear damping predicted by the diffraction potential theory is very small at this wave condition.This error was caused the theory to give the infinite response at the wave condition where it closer to semi-submersible natural frequency.

The figure 3 shown the non-dimensional heave damping calculated by diffraction potential theory, proposed viscous damping equation and the summation of both the heave damping. From the comparison, it is obtained that the heave damping calculated by diffraction potential theory increase rapidly when the wave length increase if thewavelength is below 1.5 meters. If the wavelength longer than 1.5 meters, it is obtained that the damping coefficient calculated by diffraction potential theory decrease significantly by increase the wavelength. The linear damping from diffraction potential theory finally reduced to nearly zero after wave length 5 meters. From the study, the region where the heave motion dominates by damping term is located at the location where the wave frequency is close to the structure natural frequency [21]. The heave natural frequency for this semi-submersible is located at wavelength around 9 meters. Due to the small prediction of the heave damping by diffraction potential theory, the motion response calculated in this region is becoming significant large and no agreed to the experiment result as shown in figure 4.

On the other hand, the heave viscous damping calculated by proposing equation is increasing gradually when the wave length increased. This additional heave viscous damping added into the motion equation will help to increase the damping coefficient and to avoid the large overshooting of the heave motion response when wave frequency is close to semi-submersible's heaved natural frequency.

To obtain the total damping for semi-submersible heave motion, the magnitude of damping coefficient is assumed can be directly sum up for the damping calculated by both the methods. As shown in figure 3, total damping by sum-up the executed damping between the two methods will be influenced by the damping coefficient calculated by two of the methods for the wavelength below 5 meters. However, due to the damping calculated by diffraction potential theory for this semi-submersible is trending to become zero for wavelength longer than 5 meters, then the tendency of total damping is following the tendency of the viscous damping calculated by the proposed equation. At understood the heave motion dominated by damping term is locatedin the structure natural frequency region where this region is located at wavelength around 9 meters for this selected semi-submersible model. By referring to the figure 3, the damping coefficient obtained by summing up the damping calculated by both the methods given the magnitude around 0.275.This damping magnitude was helped to avoid the motion equation to divide by zero damping then trend the motion response to infinity. At this calculated magnitude, it can be summarized that the additional viscous damping by using proposed equation can be helped to correct the damping coefficient and then corrected the motion response estimated at the damping dominated region.

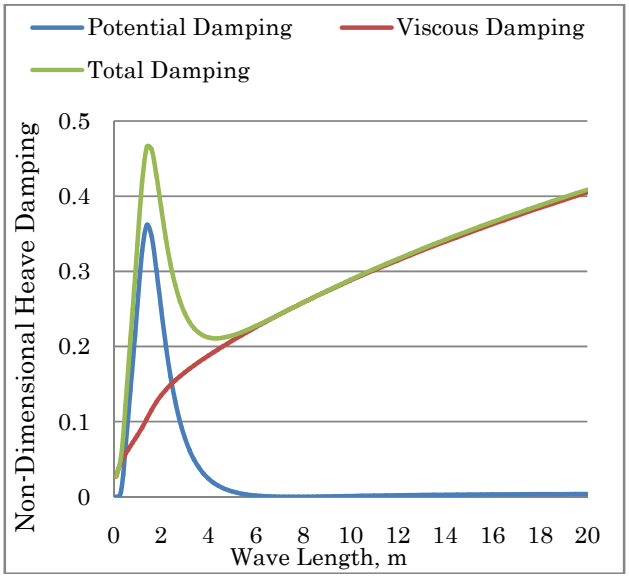

Figure 3: Non-dimensional Heave Damping for semi-submersible model

The heave RAO calculated by the diffraction potential theory and the corrected diffraction potential theory by viscous damping correction is presented in figure 4. The experimental data collected is only ranged from wavelength 1 meter to wavelength around 9 meters due to the limitation of the wave generating device in the laboratory. Comparison between the heave response calculated by diffraction potential theory with and without viscous damping correction is presented in the figure 4. From the figure, it can be obtained that the diffraction potential theory with

viscous damping correction was reduced the infinity heave response to the reasonable rangecompared tothe result obtained by diffraction potential theory without viscous damping correction.

The tendency of the heave response calculated by the diffraction potential theory with and without viscous damping correction issimilar between each other. However, due to the extra damping effect of the viscous damping correction, the heave response is no overshoot to infinity compare to results obtained from pure diffraction potential theory at wave frequency closed for the structure natural frequency (wave length equal to 9 meters). This observation also shown that a good prediction of viscous damping is significantly important to estimate the heave motion response for semi-submersible structure at damping dominates'region. Therefore, it can be summarized the neglected of the viscous effect on the estimate heave response of semi-submersible like the diffraction potential theory will lead to over prediction of heave response at the region where the motion is dominated by damping. The reason for this observation is also explained in the figure 3 where it can obtain that the damping coefficient under-predicted by the diffraction potential theory and it magnitude is almost zero at the wave condition.

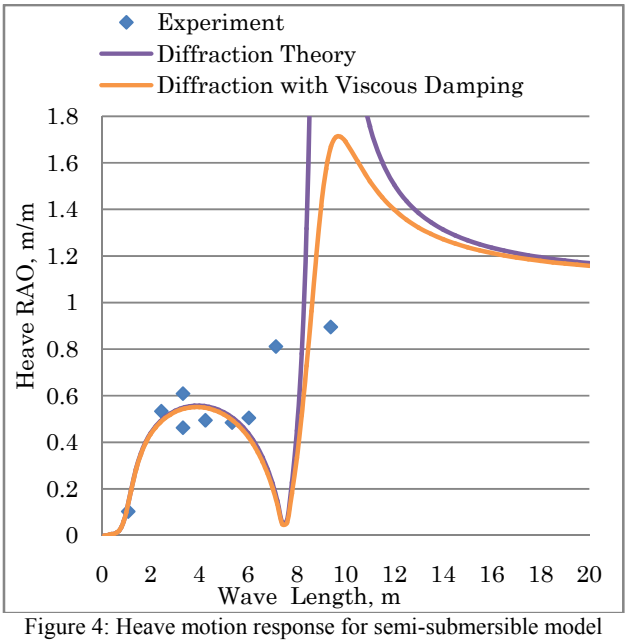

Figure 4: Heave motion response for semi-submersible model

5.0 Conclusion

In the conclusion, this paper was presented the viscous damping correction method to improve the tendency of heave response calculated by the diffraction potential theory. In general, the diffraction potential theory is a good method to predict the motion response of offshore structure especially the semi-submersible structure. In comparison to the experimental result, it is obtained that the pure diffraction potential theory isweak in predicting the heave response in the region where the heave motion is dominated by damping or drag term. The weakness of the diffraction potential theory to neglect the viscous effect was caused the damping smaller and lead to wrong heave response tendency at the damping dominated region.

By involving the viscous damping calculation using the proposed equation, the small damping magnitude calculated from diffraction potential theory can be corrected. In this paper, the numerical results calculated by the proposed method shown that the overshooting problem observed at pure diffraction potential theory had improved. At the same time, accuracy of heave motion response in head sea condition calculated by the viscous damping correction method is still agreed to experiment result. Therefore, it can be concluded that the viscous damping correction is required to consider whenthe accuracy ofthe estimated heave motion of offshore floating structure such as semi-submersible is important.

ACKNOWLEDGEMENTS

The authors would like to gratefully acknowledge to Marine Technology Center, Universiti Teknologi Malaysia for supporting this research.

REFERENCE

1 Hess, J. L., Smith, A. M. O., (1964). *Calculation of Nonlifting Potential Flow About Arbitrary 3D Bodies*, Journal of Ship Research.

2 Van Oortmerssen, G., (1979).Hydrodynamic interaction between two structures of floating in waves, *Proc. of BOSS '79. Second International Conference on Behavior of Offshore Structures*, London.

3 Loken, E.,(1981). Hydrodynamic interaction between several floating bodies of arbitrary form in Waves, *Proc. of International Symposium on Hydrodynamics in Ocean Engineering*, NIT, Trondheim.

4 Wu, S.,Murray, J. J.,Virk, G. S.,(1997). *The motions and internal forces of a moored semi-submersible in regular waves*, Ocean Engineering, 24(7), 593-603.

5 Yilmaz, A. Incecik,(1996). *Extreme motion response analysis of moored semi-submersibles*, Ocean Engineering, 23(6) 497-517.

6 Söylemez, M.,(1995). *Motion tests of a twin-hulled semi-submersible*, Ocean Engineering, 22(6) 643-660.

7 Clauss, G. F.,Schmittner, C.,Stutz, K., (2002). Time-Domain Investigation of a Semi Submersible in Rogue Waves, *Proc. of the 21st International Conference on Offshore Mechanics and Arctic Engineering)*, Oslo, Norway.

8 Matos, V. L. F.,Simos, A. N.,Sphaier, S. H., (2011). *Second-order resonant heave, roll and pitch motions of a deep-draft semi-submersible:Theoretical and Experimental Results*, Ocean Engineering, 38(17–18) 2227-2243.

9 Wackers, J. et al., (2011). *Free-Surface Viscous Flow Solution Methods for Ship Hydrodynamics*, Archive of Computational Methods in Engineering, Vol. 18 1–41.

10 Afrizal, E., Mufti, F.M., Siow, C.L., Jaswar, (2013). Study of Fluid Flow Characteristic around Rounded-Shape FPSO Using RANS Method, *The 8th International Conference on*

Numerical Analysis in Engineering, pp: 46 – 56, Pekanbaru, Indonesia.

11 Jaswar et al, (2011). An integrated CFD simulation tool in naval architecture and offshore (NAO) engineering, *The 4th International Meeting of Advances in Thermofluids, Melaka, Malaysia, AIP Conf. Proc*. 1440, pp: 1175 - 1181.

12 Abyn, H., Maimun, A., Jaswar, Islam, M. R., Magee, Bodagi, A., B.,Pauzi, M., (2012). Model Test of Hydrodynamic Interactions of Floating Structures in Regular Waves, *Proc. of the 6th Asia-Pacific Workshop on Marine Hydrodynamics*, pp: 73 - 78, Malaysia.

13 Abyn, H.,Maimun, A., Jaswar, Islam, M. R., Magee, A.,Bodagi, B., Pauzi, M., (2012). Effect of Mesh Number on Accuracy of Semi-Submersible Motion Prediction, *Proc. of the 6th Asia-Pacific Workshop on Marine Hydrodynamics*, pp: 582 - 587, Malaysia.

14 Siow, C. L., Jaswar, Afrizal, E., Abyn, H., Maimun, A., Pauzi, M., (2013). Comparative of Hydrodynamic Effect between Double Bodies to Single Body in Tank, *The 8th International Conference on Numerical Analysis in Engineering*, pp: 64 – 73, Pekanbaru, Indonesia.

15 Tiau, K.U., Jaswar, Hassan Abyn and Siow, C.L., (2012). Study On Mobile Floating Harbor Concept, *Proc. of the 6th Asia-Pacific Workshop on Marine Hydrodynamics*, pp: 224 - 228, Malaysia.

16 Kvittem, M. I.,Bachynski, E.E.,Moan, T., (2012). Effect of Hydrodynamic Modeling in Fully Coupled Simulations of a Semi-Submersible Wind Turbine, *Energy Procedia*, 24.

17 Siow, C. L., Abby Hassan, and Jaswar, (2013). Semi-Submersible's Response Prediction by Diffraction Potential Method, *The International Conference on Marine Safety and Environment*, pp: 21 - 28, Johor, Malaysia.

18 Lu, L., et al. (2011). *Modelling of multi-bodies in close proximity under water waves—Fluid forces on floating bodies*. Ocean Engineering. 38(13): p. 1403-1416.

19 Nallayarasu,S. and Siva Prasad, P., (2012). Hydrodynamic Response of Spar and Semi-submersible Interlinked by a Rigid Yoke - Part 1: *Regular Wave, Ship and Offshore Structures*, 7(3).

20 Christina Sjöbris, (2012). Decommissioning of SPM buoy, *Master of Science Thesis*, Chalmers University of Technology, Gothenburg, Sweden.

21 Journee, J.M.J and Massie, W.W. (2001). *Offshore Hydromechanics. (1st Edition.)*, Delf University of Technology.

Journal of Ocean, Mechanical and Aerospace
-Science and Engineering-, Vol.5

March 20, 2014

Preliminary Design of Archimedean Screw Turbine Prototype for Remote Area Power Supply

Erino Fiardi,[a,*]

[a)] *Mechanical Engineering Department, Bengkulu University*

*Corresponding author:riyuno.vandi@yahoo.com

Paper History

Received: 15-March-2014
Received in revised form: 18-March-2014
Accepted: 19-March-2014

ABSTRACT

This paper is aimed to design a prototype of screw turbine for power generation. Using principles of velocity vector, the governing equations have been identified for an ideal case of force acting on blade. The paper also describes the conception of a screw turbine rotor for remote area electricity production. The research is done by calculating based on theoretical way and compared with experimental results. Output power can be generated by this small size of turbine is 0.236 watt theoretically and 0.098 watt experimentally. Various losses in the system are discussed, which is also demonstrated that the experimental power outputs and theoretical predictions has a discrepancy. However, it has a great potential to be used for remote area to generated power by using low head water source as this research is developed.

KEY WORDS: *Screw Turbine; Low Head; Blade Screw; Power; Remote Area.*

1.0 INTRODUCTION

Energy crisis around the world encourage researcher to pay attention in founding another sources of green energy these days. A lot of research has been conducted by using natural energy sources such as solar, wind, wave and water. According to sources of energy from water to run a turbine, there is a rapid change of technology in using such turbine which suitable for definite kind of flow river, much of them are used for high head (differences) to produce electricity. Meanwhile, Archimedean hydro technology which had a very long history in the world [1], with various machines and mechanism, gears, pumps, various mills driven by water wheels etc. [2]. The Roman engineer Vitruvius gave a detailed and informative description of the construction of an Archimedes screw in his "De Architectura" [3]. During the last years, the inverse use of the Archimedean screw, as a kind of inverse screw pump-turbine, is under discussion within the hydropower scientific community [4-7]. Then it was started to use as Archimedean screw turbine with very low head differences of less than 2-3 metres in several years, so can be used in small river. The renaissance talking place actually throughout the world in the promotion and construction of renewable energy low-head small hydro plants valorises Archimedean screw turbines [8-10]. Such hydropower plants were installed during the last decade in Central Europe by several industrial companies, which are based on the inversion of the energy flow in their pump operation and turning the old screw pumps into new Archimedean turbines [1]. However, low head hydropower plants are developing very slowly, despite the fact that recent Archimedean screws are new type of turbines mainly in Greece but also in other countries throughout the globe [1].

Furthermore, in the rapid-change of technology these days, there is an environmental issue for saving fish and other biota on water while using water as a source of energy. As seen in several developed countries, there is a ban to dam a river that can disturb its ecosystem. There should be a consideration of how to safe them while building hydropower electricity system. Installation of Archimedean screw turbines is unlikely to have an impact on the quantity and quality of spawning and juvenille coarse fish habitat available in some areas [11, 12, 13].

In addition, Indonesia has a lot of big and small river. Especially in Bengkulu province, it has many small rivers with lower head, and this province does not have sufficient electricity. So Archimedean screw turbine one of appropriate technology can be applied there.

An interest in micro-hydropower turbine has grown year by

year. The feasibility of micro-hydropower by using axial flow turbine was examined. However, this kind of turbine has several weaknesses such as its need of high head and its lack of environmentally friendly causing fish cannot pass through that turbine blade. Because of these, another kind of turbines-Archimedean screw turbine- has attracted much attention and its practical application has been accelerated in developed countries, meeting with demand for improvements in using natural sources of energy. Due to this situation, the applications of hydropower turbine to generate electricity has been actively researched. In current practice of hydropower turbine, there is a rapid introduction of lower head kinds of turbines.

Therefore, any kind of axial flow turbines like Kaplan and Pelton have also been energetically studied. However, not only because this type of turbine is not applicable to any river on that area due to its need of high head, but also because there is no chance for fish to move along the river due to the water in the dam has to flow through the turbine. Therefore, a turbine that can eliminate such a delicate problem is highly desirable.

This paper will focus mainly in making a prototype and experimentation of Archimedean screw turbine under the micro-hydro range for low head applications. Simple manufacturing methods using locally available material will be presented. The performance of the test unit will be explored and evaluated as well as identify potential areas for improvement.

2.0 PREVIOUS WORK

Some researches already done about Archimedean screw. At first, Archimedean screw is used as a pump to raise water for irrigation and drainage [8]. Recently, researches concerning to this area are Archimedean screw has also found a new application operating in reverse as an energy converter for low head differences [17], measurements of the Archimedean as an energy converter showed the effect of inflow water level to diameter, and gave efficiencies between 79 and 84%, making this an interesting alternative for turbines in low head hydropower applications [5, 14, 17, 18], the power is generated by the hydrostatic pressure difference and the horizontal screw velocity [5,16] and blade screw.

Bengkulu province has a lot of small river with low head so that this kind of turbine can be applied. This province is still lack of electricity particularly in many remote areas. Therefore, research about Archimedean screw turbine must be done.

3.0 BASIC DESIGN

Water weight is generally assumed enclosed by the screw's blades drives the screw [14, 18]. If no losses are assumed, all potential energy contained in the flow can be extracted giving such a machine the theoretical maximum efficiency of 100%. However, most of the water weight in the Archimedean screw rests on the trough, which does not move. Power is generated by force and velocity, and since the velocity vector of the rotating screw acts tangentially to the screw, only a small part of the water weight enclosed in the screw (the part which is resting on the inclined outer section of the blade) contributes to energy conversion. Unlike the water in the cells of an overshot water wheel, weight force direction of the complete water mass coincides with the downward direction of the cell movement. The contribution of the weight force is therefore neglected.

A screw has a head difference h, a total length L and m turns of the helix with a horizontal distance l in contact with the water.

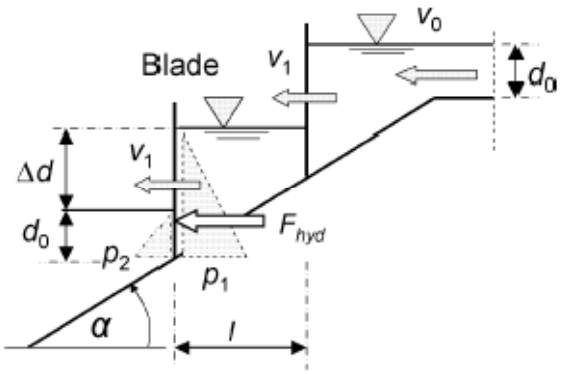

Figure1 Force acting on individual screw blade [5]

If volume and diameter of inlet pipe are known, flow rate (Q), entry velocity (v_0) and flow velocity (v_1) are :

$$Q = \frac{P}{\rho \cdot g \cdot H} = A \times V \quad (1)$$

$$v_0 = \frac{Q}{A} \quad (2)$$

The differential water levels of each blade generate a hydraulic force (F_{hyd}). While this force rotate screw with speed v_1, it can generate a power :

$$P_s = F_{hyd} \times v_1 \quad (3)$$

Trough angle (α) is relative to horizontal, a distance (l) between two individual blades makes the water depth increases by :

$$\Delta d = l \tan \alpha = (L/m) tan\, \alpha = \frac{h}{m} \quad (4)$$

So, hydrostatic force is then determined to

$$F_{hyd} = \frac{(d_0+\Delta d)^2}{2} \rho . g \quad (5)$$

Water speed in screw (flow velocity) is

$$v_1 = \frac{d_0}{d_0+\Delta d} v_0 \quad (6)$$

Power of one blade (P_{blade}) produce by multiplication of force and velocity. If there are m blades, so total power (P) will be increased. Therefore, available hydraulic power (P_{hyd}) is

$$P_{hyd} = \rho . g . Q . h = \rho . g . d_0 . v_0 . m . \Delta d \quad (7)$$

$$P_{blade} = P_{hyd} \times v_1 \quad (8)$$

$$P = m \times P_{blade} \quad (9)$$

While n = d0/Δd then theoritical efficiency η_{th} becomes

$$\eta_{th} = \frac{P}{P_{hyd}} = \frac{2n+1}{2n+2} \quad (10)$$

4.0 GOVERNING EQUATIONS

By using formulas theoretical calculation, results can be determined and the values are : flow rate (Q) is 0.00019 m3/s, inlet area (A) is 0.00114 m2, inlet speed (v_0) is 0.167 m/s, water depth increased (Δd) is 0.05 m while inlet water depth (d_0) is 0.00126 m , hydraulic force (F_{hyd}) is 6.4 N, speed of water in screw blade (flow velocity, v_1) is 0.0041 m/s. All of these values will end to get power of screw turbine (P), 0.236 Watt respectively and theoretical efficiency (η_{th}) 50 % is gotten.

5.0 EXPERIMENTAL SET UP

Screw turbine prototype is made by using locally available materials. PVC pipe with 4 in diameter is used as duct (trough), aluminum is used as screw blade and joined by using rivetted. Turbine is installed with elevation of through (α) 45^0. Two reservoirs and two pumps is used to keep flow rate constant (figure 2 and 3).

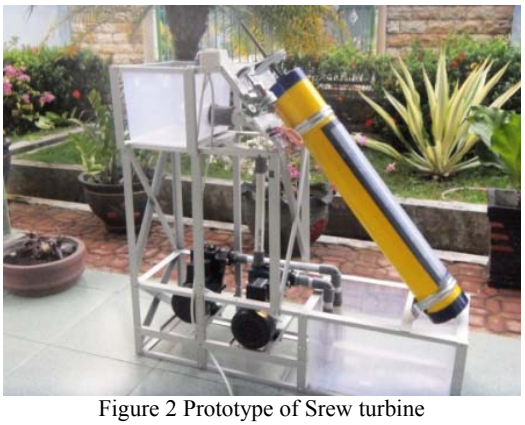

Figure 2 Prototype of Srew turbine

Figure 3 Inlet reservoir

To make sure that electricity is really generated by this device, not only some led lamps is installed on bicycle generator is on, but also measured by using multimeter to show how much current and voltage are generated. (figure 4, 5 and 6).

Figure 4 Led lamps

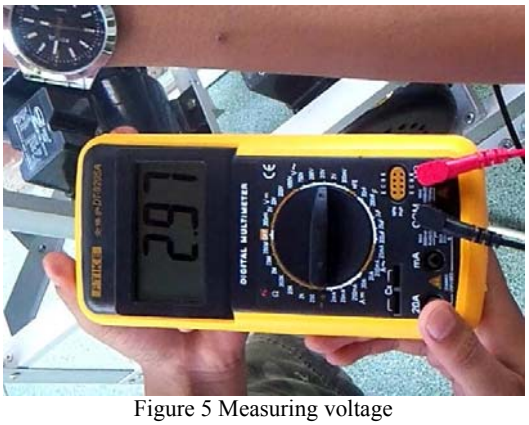

Figure 5 Measuring voltage

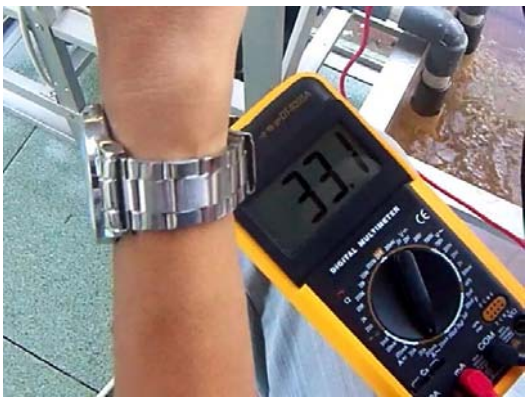

Figure 6 Measuring current

6.0 PERFORMANCE CHARACTERISTICS

By using flow rate of water (Q) 19 ml/s (0.00019 m^3/s) with inlet speed (v_0) 0,167 m/s, and also with measurement of rotation with tachometer get 232 rpm on turbine pulley and 560 rpm on

generator pulley this turbine can generate power 0.098 watt, which consist of 33.1 mA current and voltage 2.97 volt. Comparing this power with power from theorytical prediction, efficiency of this turbine is 41%. This experiment has lower efficiency than theoritical prediction (50%).

This turbine is built with locally simple materials and installed in easy way without paying attention in precision, particularly in position of generator, excentricity between generator and turbine shaft, and also tension (tight) of belt and pulley diameter. Because of lack of measurement device, torque of turbine cannot be measured. Results of this experiment is promising because better installing of this turbine should increase its performance. Furthermore, different angle of trough and blade might be taken effect on turbine performance.

.

7.0 CONCLUSION

Valuable information about the performance characteristics of screw turbine was collected through the experiments.

Screw turbine is built succesfully with locally simple material and this turbine can generate power 0.098 watt with 41% efficiency. By considering equipments and measurement tools that used, this result is promising to be continued. It should need more research to do before this turbine used in remote area.

8.0 FUTURE WORK

To get optimum parameter design, it needs to be done more research in other angle of trough and blade, and also addition on number of blade and influenced of length of blade screw.

ACKNOWLEDGEMENTS

The author would like to thank DIPA Universitas Bengkulu for funding under grant agreement no. 258/UN30.10/PL/2013. The Author also wishes to thank Afdhal Kurniawan M., Ahmad Fauzan S., Putra Bismantolo and Hendra Haryadi for the experimental support.

REFERENCE

1. Stergiopoulou, A.,Stergiopoulos, V. (2012). *Quo vadis Archimedean turbines nowadays in Greece, in the era of transition?*. Journal of Environmental Science and Engineering A 1, 870-879.
2. Stergiopoulou, A., Stergiopoulos, V. (2009). From the old Archimedean screw pumps to the new Archimedean screw turbines for hydropower production in Greece.*Proceedings of CEMEPE Conference.* Myokonos. June 21-26.
3. Stergiopoulou, A.,Stergiopoulos, V. (2009). Return of Archimedes: Harnessing with new Archimedean spirals the hydraulic potential of the Greek watercourses. *Proceedings of the Conference for Climate Change, Thessaloniki.*
4. Stergiopoulou, A.,Stergiopoulos, V., Kalkani, E. (2010).Quo vadis Archimedes nowadays in Greece? Towards modern Archimedean turbines for recovering Greek small hydropower potential. *Proceedings of 3rd International Scientific "Energy and Climate Change" Conference, Athens.*
5. Muller, G.,Senior, J. (2009).*Simplified theory of Archimedean screws*. Journal of Hydraulic Research 47 (5), 666-669.
6. Pelikan, B., Lashofer, A. (2012). *Verbesserung Der Stromungseigenschaften Sowie Planungs_und Betriebsoptimierung Von Wasserkraftschencken (Flow Characteristics Improvement and Optimization of Water Screw Turbines)*. Research Project. BOKU University, Vienna, German.
7. Nagel, G. (1968). *Archimedean Screw pump handbook*. report prepared for Ritz-Atro Pumpwerksbau GMBH Roding, Nurberg, Germany.
8. Rorres, C. (2000).*The turn of the screw: Optimal design of an Archimedes screw*. Journal of Hydraulic Engineering. 80, 72-80.
9. Stergiopoulou, A., Stergiopoulos, V.,Kalkani, E. (2011). Back to the future: Rediscovering the Archimedean screws as modern turbines for harnessing Greek small hydropower potential. *Proceedings of the 3rd International Conference CEMEPE 2011 & SECOTOX*, Skiathos.
10. Stergiopoulou, A., Kalkani, E. (2012). Investigation of the hydrodynamic behavior of innovative cochlear turbines.*12th EYE & 8th EEDYP Conference*, Patras.
11. Turnpenny,A.W.H. et al. (2001).*Risk assessment for fish passage through small low head hydro turbines*. ETSU-H/0600054/Rep.
12. Spah, H. (2001). *Fishery biological opinion of the fish compatibility of the patented hydraulic screw from Ritz Atro.* Bielfield, Germany.
13. Kibel, P., Coe, T. (2009). *Castleford mill hydro power fisheries assessment*. Devon, UK.
14. Brada, K.,Radlik, K.-A. (1996). Water screw motor for micropower plant. *6th Intl. Symp. Heat exchange and renewable energy sources.* 43-52, W. Nowak, ed. Wydaw Politecchniki Szczecinskiej, Szczecin, Polan.
15. Muller, G., Kauppert, K. (2004). *Performance characteristics of water wheels.* Journal Hydraulic Resources 42 (5), 42-48.
16. Senior, J.,Wiemann, P., Muller, G. (2008).The rotary hydraulic pressure machine for very low head hydropower sites.*Proceedings of Hydroenergia,Bled/Slovenia, European Small Hydropower Association*. 5B (1).
17. Hellman, H. D. (2003).*Gutachten zur wirkungsgradbestimmung einer wasserkraftsshnecke fabrikat Ritz-Atro [Report on determination of hydraulic screw efficiency manufactured by Ritz-Atro Ltd.]* Fachbereich maschinenbau und verfahren stechnik, Technical University, Kaiserslautern, Germany. (http://www.ritz-atro.de/2006/downloads/Wasserkraft_GB.pdf) [in German]
18. Brada, K. (1999).*Wasserkraftschnecke ermoglicht stromerzegung uber kleinkraftwerke [Hydraulic screw generates electricity from micro hydropower stations].* Maschinenmarkt Wurzburg, Mitteilung 14, 52-56. (http://www.maschinen-markt.vogel.de/index.cfm?pid=5156&pk=303) [in German]

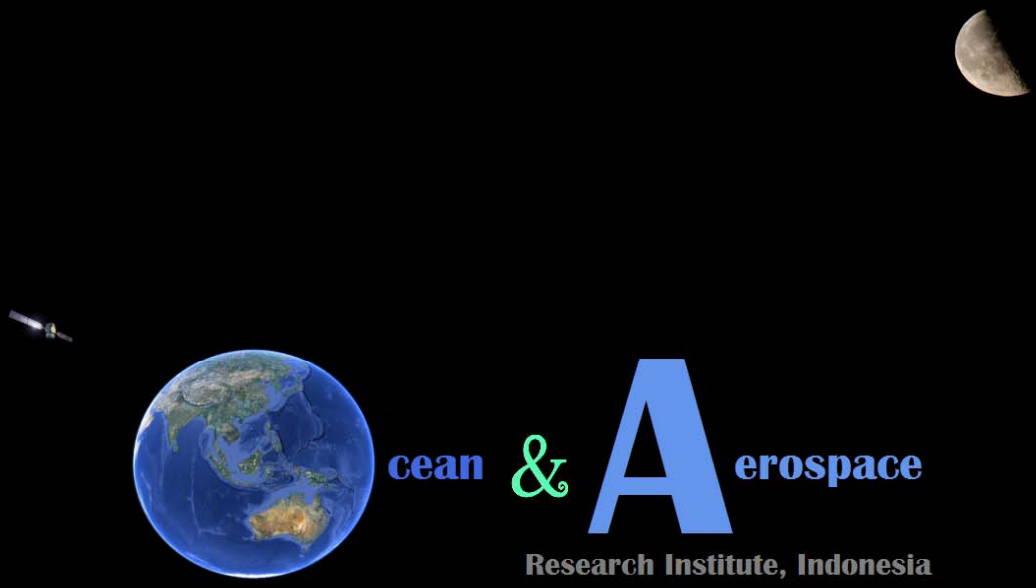

Ocean & Aerospace

Research Institute, Indonesia

UTM
UNIVERSITI TEKNOLOGI MALAYSIA
RESEARCH UNIVERSITY

Master by Taught Course

Ship and Offshore Engineering

Faculty of Mechanical Engineering
Universiti Teknologi Malaysia

Head Office

ISOMAse
Resty Menara Hotel
Jalan Sisingamangaraja No.89
28282, Pekanbaru-Riau
INDONESIA
http://www.isomase.org/

ISSN: 2354-7065